MULTI-BODY DYNAMIC SIMULATION OF LARGE DIAMETER BEARING TO STUDY THE EFFECTS OF BEARING SUPPORT PROFILE ON BEARING PERFORMANCE

By

Tenali Sudheer Reddy

ENGG02201801002

Indira Gandhi Centre for Atomic Research, Kalpakkam

A thesis submitted to the
Board of Studies in Engineering Sciences

In partial fulfilment of requirements

for the Degree of

MASTER OF TECHNOLOGY

of

HOMI BHABHA NATIONAL INSTITUTE

July, 2021

Homi Bhabha National Institute

Recommendations of the Thesis Examining Committee

As members of the Thesis examining Committee, we recommend that the thesis prepared by Tenali Sudheer Reddy titled "Multi-Body Dynamic Simulation of Large Diameter Bearing to Study the Effects of Bearing Profile on Bearing Performance" be accepted as fulfilling the thesis requirement for the Degree of Master of Technology.

	Name	Signature
Member-1	**Dr. B.K. Sreedhar** **Head, SEHD, RDTG**	
Member-2	**Dr. Diptimayee Samantaray** **Head, MFTS, MMG**	
Member-3		
Technical advisor		
Examiner	**Dr. Diptimayee Samantaray** **Head, MFTS, MMG**	
Guide & Convener	**Shri. Sriramachandra Aithal** **Head, RCAD, RDTG**	
Chairman	**Dr. A. Nagesha** **Head, FSS, MMG**	

Final approval and acceptance of this thesis is contingent upon the candidate's submission of the final copies of the thesis to HBNI.

I hereby certify that I have read this thesis prepared under my direction and recommend that it may be accepted as fulfilling the thesis requirement.

Date: 23.07.2021

Place: Kalpakkam

Signature of the Guide

Name of the Guide: Sriramachandra Aithal

DECLARATION

I, hereby declare that the investigation presented in the thesis has been carried out by me. The work is original and has not been submitted earlier as a whole or in part for a degree / diploma at this or any other Institution / University.

Sudheer
23/07/2021
Tenali Sudheer Reddy

DEDICATIONS

“A good teacher is like a candle - it consumes itself to light the way for others.”

I would like to dedicate my work to all my teachers.

ACKNOWLEDGEMENTS

I express my sincere thanks to my guide **Shri. Sriramachandra Aithal**, Scientific Officer G, Head Reactor Core and Assembly Division, IGCAR for his continued guidance and patient support throughout my project work. I am grateful to him for giving me an interesting and challenging project topic and also a benign working environment.

I would like to thank my Section Head **Shri. Gagan Gupta**, Head, Reactor Assembly Section, IGCAR for permitting me to pursue M.Tech Degree under HBNI.

I would like to express my gratitude to my M.Tech. Committee members for their valuable comments and suggestions for improvement of the work during the progress of the project. I would also like to thank HBNI for providing me the opportunity to pursue my higher studies.

I express my sincere gratitude to the staff members of BARC Training school, IGCAR campus. This project work would have never been possible without the training that I underwent in the Training school.

Sudheer 23/07/2021

Tenali Sudheer Reddy

TABLE OF CONTENTS

ABSTRACT

Large diameter bearings or slewing rings are used in Prototype Fast Breeder Reactor (PFBR) to facilitate rotation of large and small rotatable plugs for fuel handling. The performance and life of these bearings are a function of load distribution among the rolling elements such as bearing balls or rollers. Undulations – wave like deformations – forms in the large diameter bearings due to elastic deformation of bearing supporting structure, manufacturing errors and differential thermal expansions along the bearing races occurring during reactor operation. These undulations adversely affect the load distribution in the bearing resulting in non-uniform load distribution among the rolling elements during rotation of the bearing.

An estimation of the load distribution during bearing operation will help in assessment of bearing performance and life. Towards this, a Multi Body Dynamic (MBD) simulation is carried out. Performing MBD simulation of the large diameter bearing is a novel approach to study the effects of undulations and differential thermal expansions on bearing performance as no open literature is available on a similar study. With this approach load distribution in the bearing, kinematics and dynamics of rolling elements motion during bearing rotation is studied which is not feasible by conventional static finite element analysis approach.

A general purpose commercial multi body dynamic simulation tool – Recurdyn - with capability to simulate flexible bodies is used to study the effect of undulations on bearing performance. In this study, maximum load taken by the bearing balls under the individual influence of undulations and differential thermal expansions as well as the combined influences were estimated. Along with these estimates, spacer ball to load ball interaction forces during bearing operation are also estimated.

Estimated maximum loads on the bearing balls are used to estimate the fatigue life of bearing to study the effect of undulations on the bearing performance. These estimates provide inputs to make design recommendations for PFBR large diameter bearings.

LIST OF FIGURES

LIST OF TABLES

LIST OF NOTATIONS

F	=	Force on the Bearing
K	=	Contact of Stiffness of Ball to Race Contact
C	=	Damping coefficient of Ball to Race Contact
N	=	Contact Force on Bearing Race
F_f	=	Contact Friction Force on Bearing Races
δ	=	Penetration between Ball and Bearing Race Contact Surfaces
n	=	Exponent to Introduces Nonlinearity in Hertzian Contact
μ	=	Coefficient of Friction
μ_s	=	Coefficient of Static Friction
μ_d	=	Coefficient of Dynamic Friction
v_s	=	Static Threshold Velocity
v_d	=	Dynamic Threshold Velocity
L_{10}	=	Fatigue Life of Bearing with 90% Reliability
A_{cd}	=	Fatigue Life Correction Factor for Case Hardness Depth
D_b	=	Diameter of the Bearing Ball
Z	=	No of Load Balls in Bearing
α	=	Contact Angle of Bearing
b_m	=	Factor to consider improved material and manufacturing methods of bearing in ISO 281-2007 Standard
f_c	=	Factor considering the errors in mounting and manufacturing of bearing in ISO 281 code.
L_{10}	=	Life of bearing with 90 % Reliability
C_s	=	Dynamic Rating of Bearing

CHAPTER 1

INTRODUCTION

1.1 Introduction to Large Rotatable Plug (LRP) Bearing and Small Rotatable Plug (SRP) Bearing

Nuclear energy is one of the important sources of energy throughout the world. Safety of nuclear reactors is an important factor for public acceptance of nuclear power owing to the risk of radio activity release to the environment in case of any severe accidents. Currently, Generation IV (Gen. IV) reactors are meeting the highest nuclear safety standards. Out of six concepts in Gen. IV reactors, three are fast spectrum reactors. They are Sodium-cooled Fast reactor (SFR), Lead-cooled fast reactor (LFR) and Gas-cooled Fast Reactor (GFR). Owing to the advantages of nuclear safety and the breeding capability of SFR, a Prototype Sodium Cooled Fast Breeder Reactor (PFBR) is being constructed in Kalpakkam, Tamil Nadu to meet the rapidly growing energy demands of India.

Prototype Fast Breeder Reactor (PFBR) is 500 MWe sodium cooled pool type reactor. The reactor is having three main heat transport circuits namely primary sodium, secondary sodium and steam-water systems circulating primary sodium through the core. The primary sodium then transfer heat to the secondary sodium in intermediate heat exchangers. The secondary sodium heats up the water in the steam generators to generate steam for running steam turbines to produce electric power. The entire reactor internals including core and primary sodium circuit are contained in a single vessel called main vessel (MV). The top shield forms the top cover for the MV and consists of roof slab (RS), Large Rotatable Plug (LRP), Small Rotatable Plug (SRP) and control plug (CP). The top shield provides the thermal and biological shielding against the hot & highly radioactive sodium pool to facilitate personnel access to it. LRP and SRP are provided one within the other at the center of roof

slab. SRP supports control plug, Transfer arm (TA) and portion of top shield platform over SRP which in turn is supported on LRP. The fuel handling is accomplished by combined rotation of LRP, SRP and the transfer arm (TA). With the combined rotation, it is possible to access all the subassemblies located within the handling diameter thereby enabling the in vessel transfer of the subassemblies from their respective location to storage locations and vice versa. To enable rotation of LRP and SRP, they are supported by large diameter ball bearings called as slewing rings. As the name suggests these bearings with integral drive gear arrangement for the rotation, are meant for slewing operations i.e., oscillatory type of movement. Reactor assembly and rotatable plug assembly are shown in Figures 1 and 2 below.

Slewing ring bearings are rolling element bearings that typically support a heavy but slow-turning or slow oscillating loads in combination of axial, radial and moment loads. The difference between these types of bearings and the normal bearings, which are commonly used, is that they have higher pitch diameter, high load carrying capacity, large size of rolling elements, the nature of load carried – mostly static, and speed of operation. These bearings are widely used in cranes, wind turbines, heavy machinery, large antennas, etc. A slewing bearing comprises of top ring, bottom ring, rolling elements (balls or rollers), a cage or spacer to space the rolling elements so as to prevent their accumulation and a gear drive system integrated with the bearing. Their diameters range from 0.1 to 18 meter depending on the application. A typical slewing ring bearing is shown in Figure 3.

The bearings selected for PFBR are “Angle Contact Thrust Slewing Ring Ball Bearings” in order to withstand both the axial and radial load. Load balls are separated by spacer balls to prevent rubbing against each other during rotation of bearing. Spacer balls have little less size to prevent its contact with top race and thus able to rotate freely in a direction opposite to that of load balls and thereby preventing rubbing with the load balls.

This is pictorially shown in Figure 4, where spacer ball is rolling in direction, which is opposite to that of load ball.

There are two such large bearings in PFBR, one each for rotation of LRP and SRP. Representative figures showing the LRP bearing and its support structure are shown in Figures 5.

1.2 Problem Statement and Objectives

The performance and life of large diameter bearings is a function of load distribution among the rolling elements – bearing balls or rollers – which in turn depends on the bearing profile, rigidity of the bearing support structure and the temperature gradients along the bearing circumference. Undulations – wave like deformations – forms in the large diameter bearings due to elastic deformation of bearing supporting structure, manufacturing errors and differential thermal expansions occurring during reactor operation. These undulations adversely affect the load distribution in the bearing resulting in few load balls experiencing large amount of load to low or no load during its rotation in bearing. An estimation of the load distribution in the bearing under operational condition will help in assessment of bearing performance and life. Towards this, a Multi Body Dynamic (MBD) simulation is carried out to study the effect of undulations on the bearing load distribution.

Following are the objectives of the work.

1. To validate commercial multi-body dynamics (MBD) software – Recurdyn – to perform dynamic simulation of large diameter ball bearing.
2. To study the effect of undulations formed by elastic deformation of bearing support structure on the load distribution in the bearing.
3. To study the effect of undulations formed by circumferential temperature gradient on the load distribution in the bearing.

4. To study the combined effect of both the differential thermal expansions and undulations on the load distribution of the bearing.
5. Estimation of fatigue life under the above estimated load distributions to study the effect of undulations and differential thermal expansions on bearing performance.

Support structure undulation assumed in the study is plotted in Figure 6 whereas Figure 7 shows the schematic view of bearing bottom race with undulations geometrically modeled.

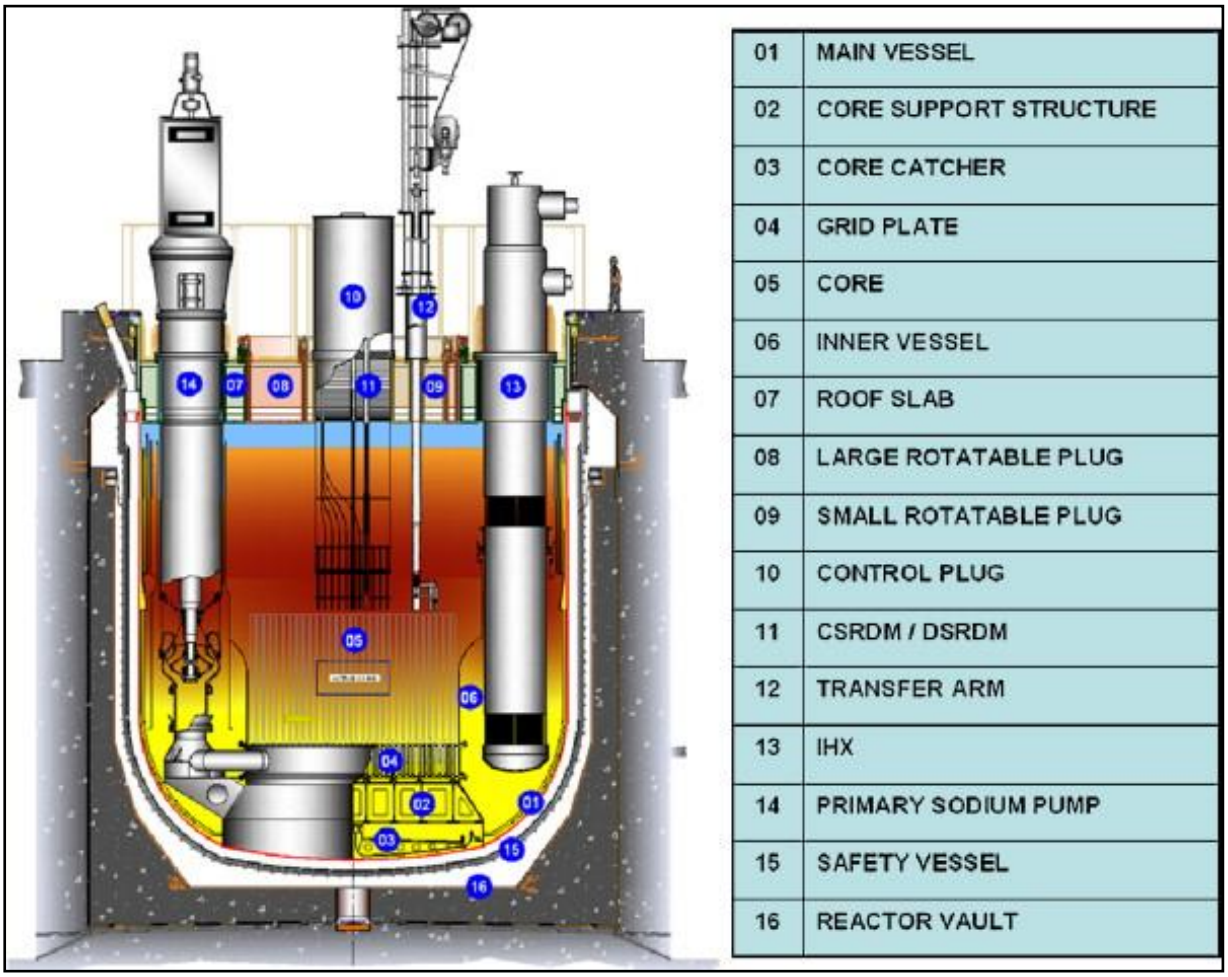

Figure 1: Prototype Fast Breeder Reactor Assembly

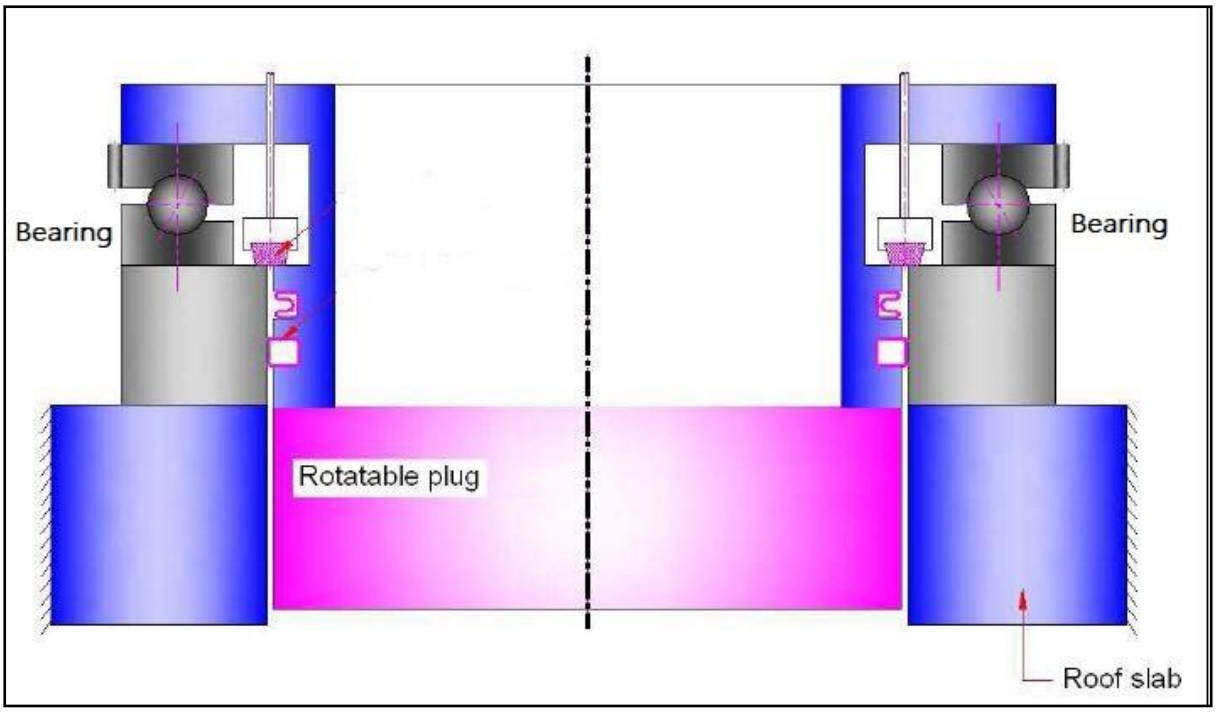

Figure 2: Sectional View of Rotatable Plug Assembly

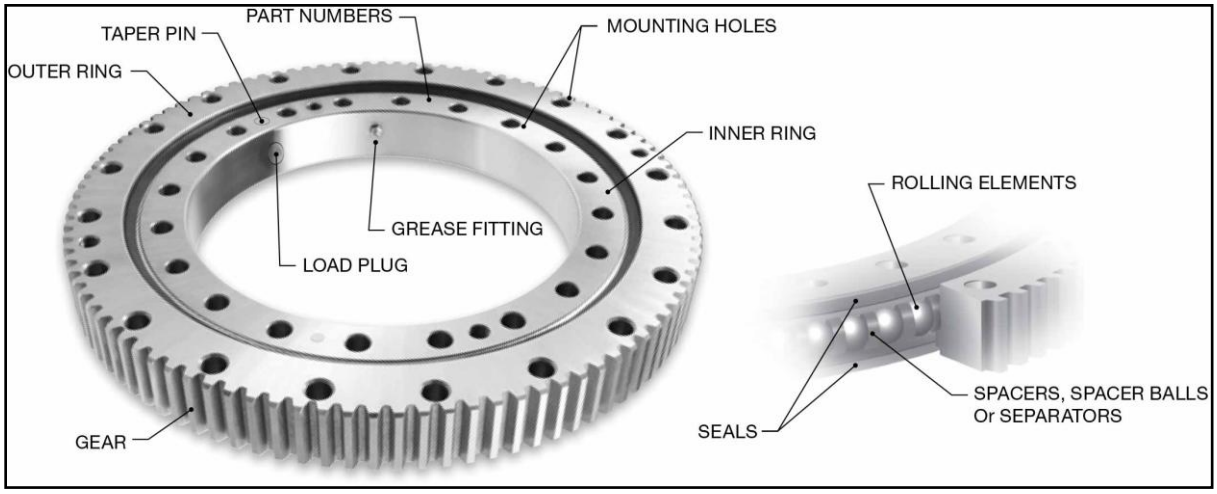

Figure 3: Large Diameter Bearing / Slewing Ring

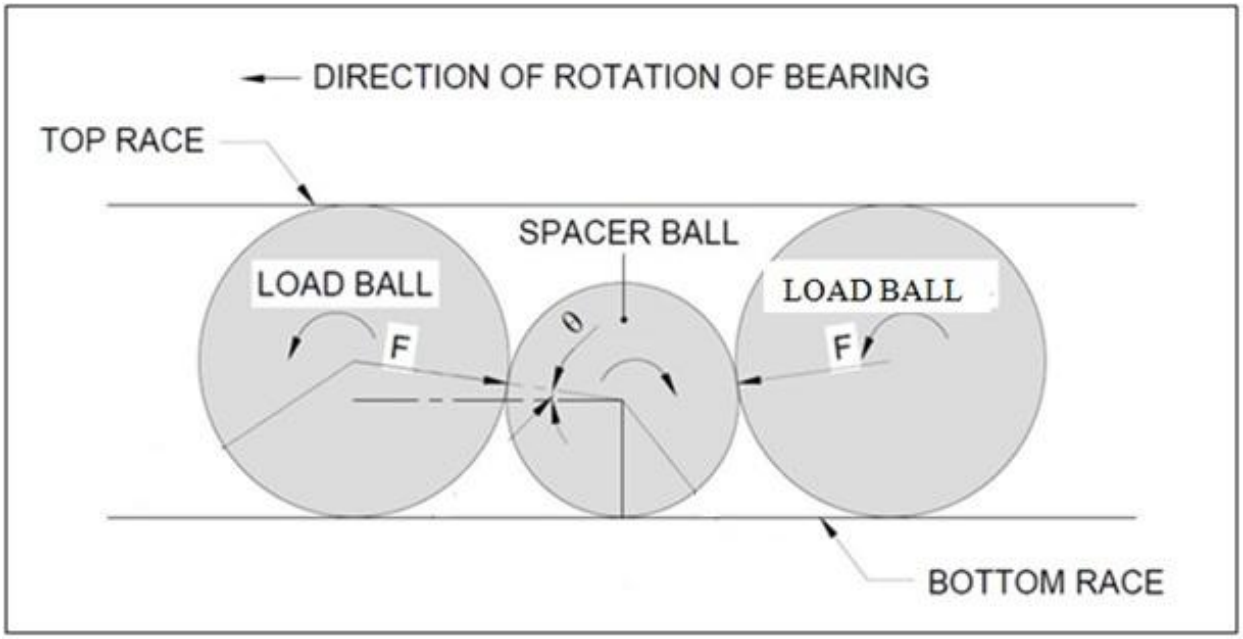

Figure 4: Load Ball and Spacer Ball Configuration

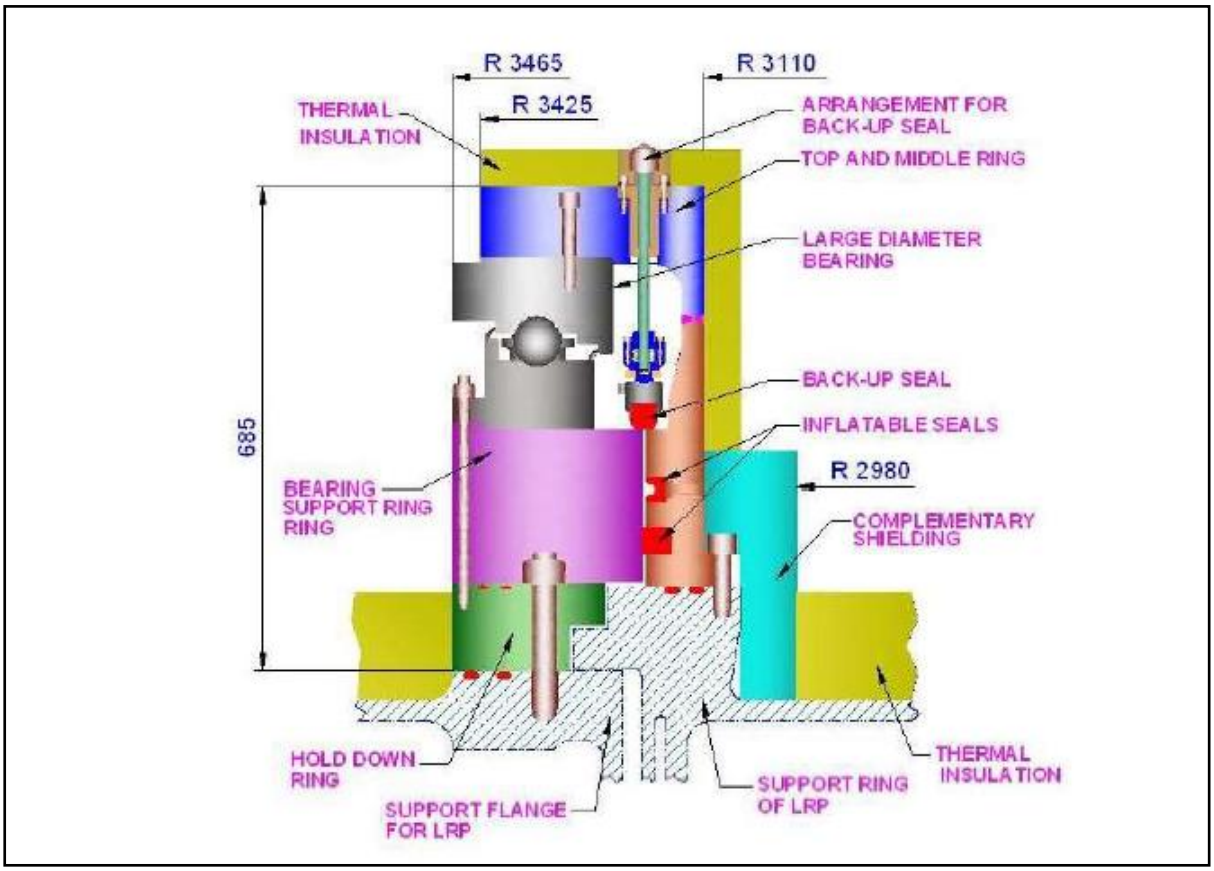

Figure 5: LRP Support Structure

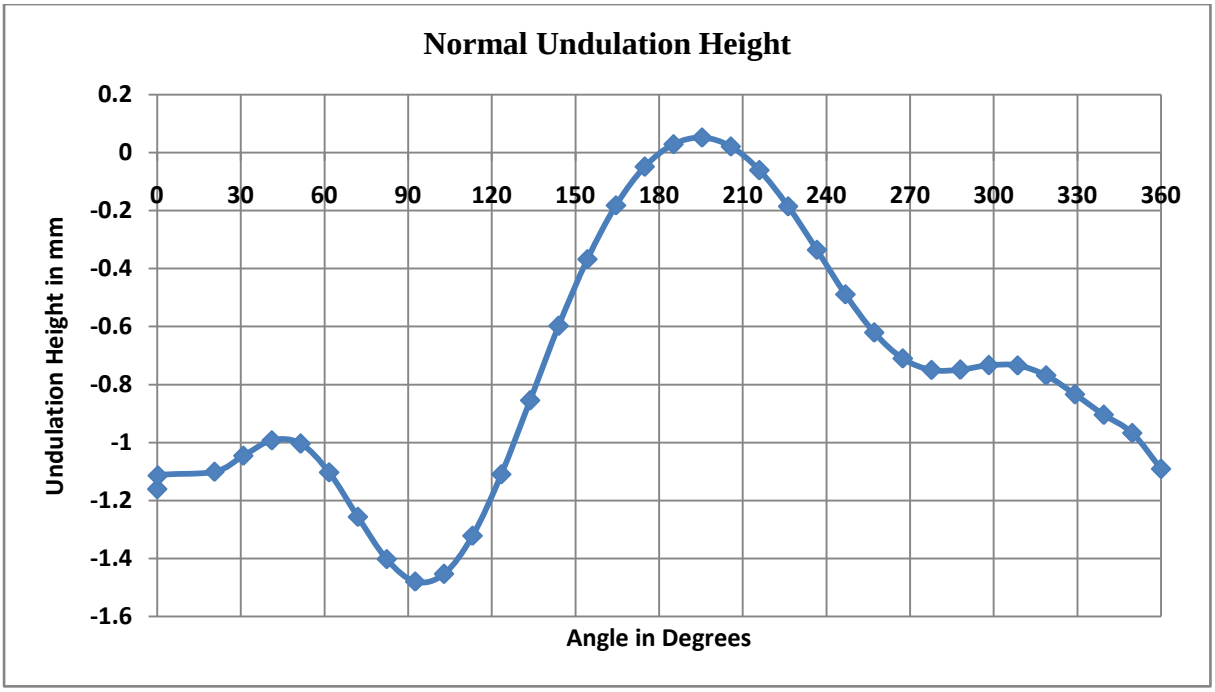

Figure 6: Undulation Profile Assumed for Study

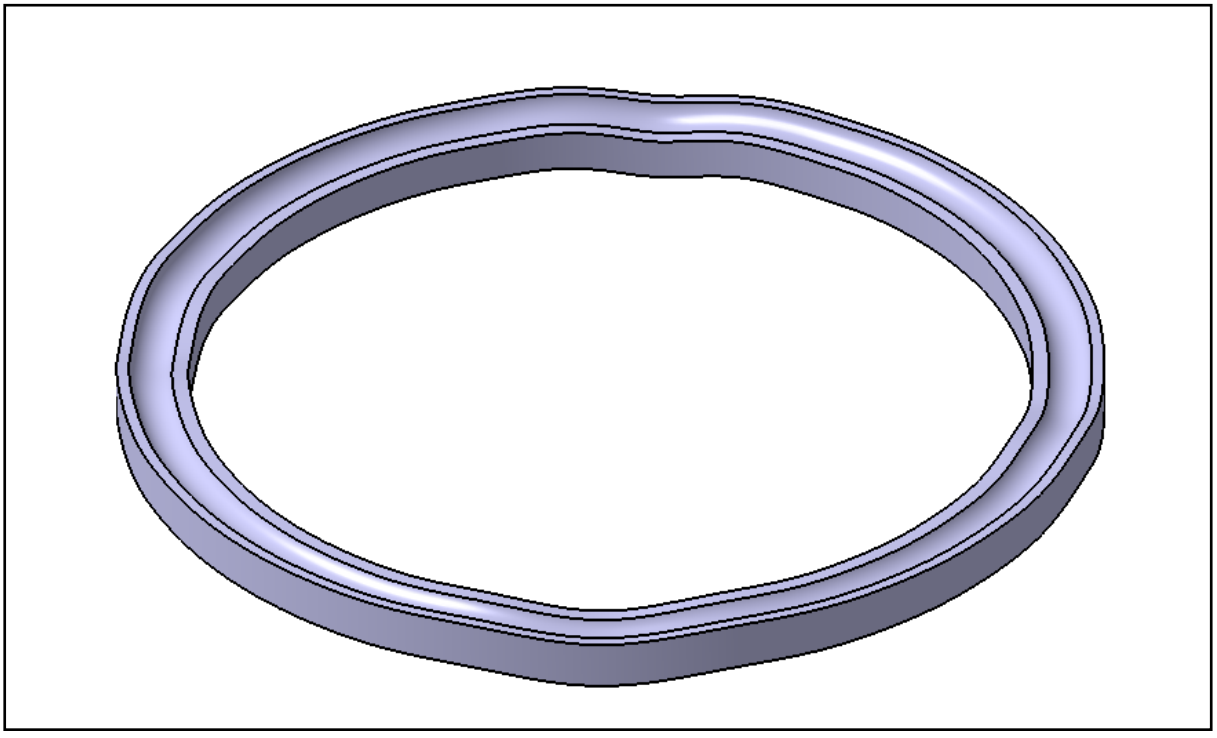

Figure 7: Bottom Race of ϕ 2m Modelled with Assumed Undulations

CHAPTER 2

LITERATURE SURVEY

2.1 Introduction

Ball bearing is a machine element used to reduce drive torque required to rotate a component with respect to other by reducing the friction between the components. Bearings can be broadly classified as rolling contact bearing and sliding contact bearings. Sliding contact bearings makes use of hydrodynamic fluid layer formed between rotating and stationary components to reduce the drive torque whereas in rolling contact bearings, rolling elements such as ball or rollers are used to reduce the drive torque by using the principle of rolling friction. Large diameter ball bearing is an anti-friction bearing used in applications where bearings are subjected to large thrust loads combined with radial and moment loads and rotate at low rotational speed. The performance of large diameter ball bearing is mainly dependent on the maximum load acting through a rolling element in the internal load distribution among the rolling elements. Maximum load on the rolling element is an input to obtain the rolling element size, bearing race case hardness depth, fatigue life etc. Many efforts are made in the last three decades to study the factors effecting the load distribution in the bearing. Some of these studies are summarized below.

2.2 Hertzian Contact Theory of Elastic Contact

Herzian contact theory deals with the contact parameters such as contact pressure, contact deformation, dimensions of contact region when two solids are pressed against each other. The contact between the bearing ball and bearing race can be modeled as a Hertzian contact with following assumptions. [1]

1. All contact deformation occurs in the elastic range and it follows the Hooke’s Law.

2. The contact load is perpendicular to the surface, that is, the contact surfaces are perfectly smooth and the friction force at the surface is neglected.
3. Size of the contact area is much smaller compared with the curvature radii of the contact bodies.

Detailed procedure to calculate contact pressure and deformation are presented in reference 1. In a Hertzian contact, the solids subjected to contact will develop stress at the sub surface region. These sub-surface contact stresses are responsible for the contact fatigue of bearing races. Detailed calculation methodology to obtain maximum sub-surface shear stress in Hertzian contact for a given load and geometry are presented by Thomas and Hoersch [2]. This method is briefly discussed below.

$$Maximum\ Shear\ Stress = \frac{1}{2}(S_z - S_y)$$

$$S_y = \left(M\left(\Omega_y + v\Omega_y^{'}\right)\right)\left(\frac{a}{\Lambda}\right)$$

$$S_z = \left(\frac{M}{2}\left(\frac{1}{\eta} - \eta\right)\right)\left(\frac{a}{\Lambda}\right)$$

$$M = \frac{2k^2}{e^2 E(e)}$$

$$\eta = \sqrt{\left(\frac{k^2 + k^2\left(\frac{z}{b}\right)^2}{1 + k^2\left(\frac{z}{b}\right)^2}\right)}$$

$$\Omega_y = \frac{1}{2\eta} + \frac{1}{2} - \frac{\eta}{k^2} + k\left(\frac{z}{b}\right)\left[\frac{1}{k^2}E(\phi, e) - F(\phi, e)\right]$$

$$\Omega_y^{'} = -1 + \eta + k\left(\frac{z}{b}\right)[F(\phi, e) - E(\phi, e)]$$

Where,

S_z= Principle stress in the direction normal to Hertzian contact

S_y = Principle Stress in the direction normal to rolling direction

b = Length of semi-minor axis of elastic deformation

a = Length of semi-major axis of elastic deformation

z = Normal depth from raceway surface

k = Contact Modulus = b/a

$e = \sqrt{(1 - k^2)}$

$\phi = \tan^{-1}\frac{a}{z}$

$E(e) = \int_0^{\frac{\pi}{2}} \sqrt{1 - e^2 \sin^2\theta}\ d\theta$ (Complete Elliptical Integral of Second Kind)

$F(\phi, e) = \frac{1}{\int_0^{\phi} \sqrt{1-e^2 \sin^2\theta}}\ d\theta$ (Incomplete Elliptical Integral of First Kind)

$E(\phi, e) = \int_0^{\phi} \sqrt{1 - e^2 \sin^2\theta}\, d\theta$ (Incomplete Elliptical Integral of Second Kind)

Above method is used to obtain sub-surface shear stress profile for a given load on the bearing ball. Computer program developed for the above method is presented in Annexure-I.

2.3 Factors Influencing Load Distribution in the Bearing

Failure modes of large diameter ball bearings is discussed in detail in the document "Bearing Damage and failure Analysis" presented by SKF Bearings [3]. In this document, various causes of ball bearing failures such as excessive load on bearing balls, contamination, lubrication failure, plastic indentation, and misalignments are discussed in detail.

The influence of supporting structure stiffness on the ball bearing load distribution is presented in the work of Zwirlein et al. [4]. Load distribution in the slewing ring of bucket wheeled iron ore mining equipment is presented in this study by considering the elastic

deformation of its supporting structure. Based on the maximum load on the rolling element, static capacity is calculated.

In the work of Tadeusz et al. [5], the effect of supporting structure stiffness of slewing bearings is discussed. It is stated that obtaining a uniform load distribution in the bearing is difficult to achieve due to the flexibility of the supporting structures in mining equipment and other earth moving machines. Further assessment of bearing and its component's life dependency on the ball bearing load distribution is discussed.

Effect of manufacturing errors on the load distribution in large diameter bearings for nuclear reactor applications is presented in the work presented by Aithal et al. [6]. FEA based approach is used to study the influence of waviness height and spacing on the load distribution in the bearing. In this study, a sector of bearing along with bearing balls is modeled using solid elements.

A detailed large diameter ball bearing failure is described by Ost W et al. [7], due to the uneven load distribution in a dockside crane bearing. The large diameter bearing used in the equipment failed earlier than its estimated fatigue life by spalling of bearing races at the high load locations. Root causes for the early failure are identified and non-uniform bearing support structure stiffness is identified as the major culprit.

Effect of load distribution on life of radial roller bearing under the influence of elastically deformed bearing races is presented by Nagatomo et al. [8]. It is observed that the fatigue life of the bearing reduced considerably under the influence of uneven load distribution produced by the deformed bearing races.

Effect of irregular geometry on the load distribution and the fatigue life of double row slewing ball bearing are presented by Potocnik R, et al. [9]. A fatigue life calculation method for bearings with induction hardened races is also presented to show that the irregular geometry will decrease the bearing life. Further Potocnik R, et al. in ref. [10]

presented a method to calculate static capacity of the bearing with irregular geometry. Under the irregular geometry, static capacity of the bearing is shown to decrease considerably.

As large diameters bearings are operated at low speed, effect of heat generation and temperature gradients is not studied extensively in literature. Following are few literatures studying heat generation and the effects of temperature rise in small radial ball bearings.

Influence of thermal deformation of bearing on the performance of helical gear supported on it is studied by Liu X et al. [11]. By using static and quasi-static analysis methods, performance of gear is obtained under the influence of thermal expansion in the bearing. But not much is discussed on the effects of thermal expansion on the performance of bearing.

Effect of thermal expansion in small angle contact radial bearing races is studied by Mitrovic et al. [12] using FEA simulations. Effect of operation temperature on the load distribution, contact stiffness of bearing race and clearances are studied. Based on the study, it is concluded that rise in bearing operation temperature resulted in increase in the bearing load due to increased contact angle between the bearing balls and the race. This resulted in reduced fatigue life of the bearing.

2.4 Modeling Techniques to Estimate Load distribution in Bearing

Design of support structures to mount large diameter bearings without any elastic deformations is a challenging task. So, these bearings are mounted on relatively flexible structures when compared to small bearings. Supporting structures of these large diameter bearings are subjected to elastic deformations due to heavy load transferred from the bearing as well as due to connected loads to the structure. These elastic deformations results in undulation formation in the bearings. Various analysis methods are developed to estimate

load distribution among the rolling elements under the influence of undulations. Some of these methods are discussed below.

Kania L et al. [13] performed a 3D finite element simulation to estimate the internal load distribution in bearings. In this model, races are modeled by 3D solid elements and balls are modeled as non-linear beam elements. Though this method simulates the effects of undulations, it is limited to static analysis and dynamic effects such as friction acting on the bearing balls cannot be simulated.

X H Gao et al. [14] also used FEA model to estimate load distribution in the bearings under the influence of undulations using non-linear springs. In this method, undulations in the bottom race are modeled as per the elastic deformations of supporting structure. Non-linear springs representing the stiffness of Hertzian contact between the ball and races are connected between the top and bottom race. The top race is modeled as a flexible body with load acting on its top surface in order to account for the deformation of the race. Since, non-linear springs are used instead of beam elements as in Kania's model [13], the ball to race contacts are better represented.

Both of these FEA methods discussed above are limited to static analysis and can't be used to predict the dynamic behavior of balls under the influence of undulations. Moreover, these methods cannot be used to estimate ball to ball interaction forces and the effects of misalignments in bearing raceways formed due to thermal expansions. To overcome these limitations in the study on effects of undulations and differential thermal expansions, a flexible multi body dynamic (MBD) analysis of the bearing is proposed.

2.5 Estimation of Fatigue Life of Large Diameter Bearing

Damage of large, slowly running bearings is caused mainly by static loads and material fatigue. Damage caused due to material fatigue is considered in estimating dynamic capacity and L_{10} life (life of bearing with 90% reliability) of the bearing using ISO 281[15]

standard. Calculation of L_{10} life of the bearing as per ISO 281-2007 standard is presented below.

1. Calculation of Dynamic Rating of the Bearing (C_a)

   Dynamic load rating means the load at which the bearing rotates for one million rotations with 90% reliability.

$$C_a = 3.647 b_m f_c (cos\alpha)^{0.7} \tan\alpha \, Z^{\frac{2}{3}} D_b^{1.4} \qquad \text{Eq. 2.1}$$

   Where,

   D_b = Diameter of the Bearing Ball

   Z= no of load balls

   α = Angle of bearing

   b_m = Factor to consider improved material and manufacturing methods of bearing races

   $f_c = Value\ obtained\ from\ the\ Table$ 4 of ISO 281 code.

2. Calculate ISO bearing fatigue life using equation below

$$L_{10}\ life = \left(\frac{C_a}{P_a}\right)^3 \qquad \text{Eq. 2.2}$$

But this standard pertains to bearing manufactured from AISI 52100 steel through hardened to at least a minimum of 58HR_C. So, an estimate of fatigue life of the bearing considering case hardness profile of the bearing is necessary. Based on the "Wind Turbine Design Guidelines DG03: Yaw and Pitch Rolling Bearing Life" given by National Renewable Energy Laboratory (USA) [16], an estimate of fatigue life of LRP bearing is calculated.

As per the Ref.16, procedure to calculate fatigue life of large diameter bearing with induction hardened raceway is mentioned below.

1. Calculate fatigue life (L_{10} life) of bearing as per ISO 281.

2. Calculate subsurface shear stress profile at the Hertzian contact between bearing race and ball at maximum rolling element load.
3. Indentify effective case depth (where 50 HR_C is reached) of the raceway as per its hardness profile.
4. Calculate shear stress at 110% of effective case depth.
5. Calculation of fatigue strength of core material.

$$\text{Yield Strength in Shear} = 0.425 \times \text{UTS of core material}$$

$$\text{Fatigue Strength in Shear} = 0.6 \times \text{Yield Strength in Shear}$$

6. Multiply the ISO 281 L_{10} life with a factor A_{cd} to obtain fatigue life of bearing with case hardened race.

$$A_{cd} = \frac{\text{Allowable Shear Strength}}{\text{Contact Shear Stress at Hardened Case to Core Material Interferance}}$$

Correction factor A_{cd} is used to correct the fatigue life calculated by ISO method.

2.6 Multi-Body Dynamic Analysis of Bearing

Literature published on multi-body dynamic (MBD) analysis mostly deal with the mathematical modeling of 2D ball bearing simulations to study the effect of radial and eccentric axial load on load distribution in radial deep groove bearings [17-19].Open literature available on 3D MBD analysis of bearing is very limited and moreover, no open literature exists on flexible MBD analysis used to study undulation effects on load distribution in ball bearing.

Multi-body dynamics (MBD) analysis simulates the motion of individual elements of a machine subject to its kinematic constraints and forces applied. There are mainly two MBD programs developed for the analysis of bearings, BEAST developed by SKF bearings [20] and ADORE developed by Pradeep K Gupta. [21]

BEAST (BEAring Simulation Tool) developed in-house by SKF Engineering and Research Centre for their internal use to assess the performance of new bearing designs. This is a multi body dynamics simulation tool specific to bearing applications. All bodies (races, balls, cage) are modeled with 6 degree of freedom (DOF) subjected to appropriate kinematic constraints and loads imposed on them. This tool is capable of predicting the contact path of bearing balls, load distributions, interaction force between the balls and cage using less computational resources when compared to traditional MBD programs. As it is a proprietary tool developed for the internal product development of SKF bearings, it is not possible to obtain the tool. Moreover no open literature is available on its application to slewing ring thrust bearing simulations.

ADORE (Advanced Dynamics of Rolling Elements) is a dedicated rigid body dynamics simulation software developed by Pradeep K Gupta. It is commercial software intended to estimate bearing performance parameters such as life, heat generation, wear of various elements, torque variation, instability of motion of cage, load on rolling elements. The classical differential equations of each bearing element, including rolling elements, cage and races, are formulated in a generalized 6 DOF system, while applied forces and moments are derived from mathematical models for interacting bearing elements. However, this tool is not suitable for the current study as it cannot simulate flexible bodies as the study of undulation effects requires the modeling of top race and top and middle ring as flexible bodies to simulate race deformation.

Due to the lack of availability of dedicated bearing dynamic simulation programs with flexible MBD simulation capability, general purpose commercial multi body program – Recurdyn [22] –was employed in the current study to estimate load distribution in large diameter bearings. Recurdyn, general purpose MBD software with features to simulate flexible bodies is selected because of its advanced features such as FEA and component

modal synthesis (CMS) based flexible bodies, user friendly rigid body to flexible body contact modeling, inbuilt geometric modeling module, inbuilt meshing module and advanced graphics visualization.

2.7 Flexible Bodies in Multi-Body Dynamic Analysis [22]

Recurdyn supports modeling of deformable bodies by two methods, one by traditional Finite Element Method (FEM) and the other by Component Modal Synthesis (CMS) methods. The traditional FEA based deformation bodies modeling is called as FullFlex and CMS based modeling is called as Reduced Flex. Here reduced means reduction in the computational complexity.

In CMS method the mode shapes of vibration are calculated as per constrains applied on it. In CMS method, specifically Craig and Bampton formulation, modes are used in conjugation with the component level masse and stiffness matrices to generate reduced mass and stiffness matrices used in finite element analysis. Thus the computational intensity involved in the full flexibility model i.e., FEA based model is reduced. The limitation on CMS modeling is that it can be used to model in linear structural deformation.

CHAPTER 3

MODELING DETAILS AND VALIDATION OF GENERAL PURPOSE MBD SOFTWARE TO PERFORM DYNAMIC ANALYSIS ON LARGE DIAMETER BEARINGS

A general purpose multi body dynamics tool – Recurdyn – with features to model flexible bodies is chosen for the large diameter bearing analysis. Prior to modeling the actual problem, validation of the tool to handle the problem in an accurate way is recommended. Experimental validation is the most preferred mode. However, extracting and co-relating the experimental data for a problem like load distribution in large bearing is not yet studied. The next option is to carryout benchmark studies with published literatures. Here also, there are no published literatures which could be used for a dynamic problem as all such published data related to static analysis. Hence, to carryout validation of the Recurdyn software to simulate large diameter bearings to obtain load distribution among the bearing balls under the influence of undulations, following validation process is evolved and followed:

1. Validation of static analysis
2. Validation of dynamic analysis
3. Comparison with Finite Element Method(FEM) and Component Modal Synthesis(CMS) flexibility formulations
4. Validation of dynamics solver to study effects of bearing undulations

Initially the MBD tool is validated by performing a static simulation on the bearing with only axial load acting at the centre of the bearing with zero eccentricity. This analysis is validated against analytical solution both for rigid and flexible multi-body simulations. After validating static analysis, a dynamic simulation is performed by rotation of bearing top race to obtain the load distribution among the bearing balls during rotation of bearing race. This

load distribution is validated against the analytical solution. These two validations helped in gaining confidence in the modeling details used in the simulation.

In order to further validate the tool to check its suitability to study the effects of undulations, a MBD simulation with undulation profile (shown in figure 6) modeled in the bearing bottom race and top race modeled as flexible race is performed. Load distributions in static and at one particular instance of time during dynamic simulation matching the static configuration of bearing are compared to validate the MBD results. As static and dynamic simulation results are closely matching with each other there is enough confidence on the results to use the tool in the study.

3.1 Description of Modeling and Analysis of Large Diameter Bearing Using Recurdyn

Modeling of large diameter bearing in Recurdyn involves modeling of geometric bodies, constraints, contacts and solver selection. Following are the steps involved in modeling a problem in Recurdyn.

a) Geometric and Material Modeling

This is the first step in the modeling. It involves geometric modeling of the bearing in the dedicated geometric modeling module inside Recurdyn or one can alsoimport geometric models from other computer aided design (CAD) software in formats such as igs, stp, catpart, catproduct, etc., Flexible bodies are modelled by meshing the imported geometric models in the inbuilt meshing model. The mesh tool supports beam, shell and solid elements in flexible bodies. Material properties such as density, Young's modulus and Poisson's ratio are assigned to geometric models.

Geometric modelling details of the large rotatable plug are presented below in table 1 [23] below. The large diameter bearing under consideration is modelled as per the bearing profile shown in Figure 8. It is an angular contact thrust bearing with a contact

angle of 60°. Along with the bearing, bottom support structure and top and middle ring (shown in Figure 5) are modelled. Bottom support structure is labelled as ground i.e., it acts as the base for rest of the bearing assembly. All the bodies are assigned with the steel material properties by default.

Recurdyn supports both rigid and flexible bodies. Rigid bodies do not support deformation of parts during simulation where as the flexible body support deformation. In order to study the effects of undulation on the bearing performance, top race and TMR are modelled as flexible bodies as the beading of top race and TMR effect the load distribution.

Table 1: MBD Simulation Geometric Model Details

Body	Description
Bearing Rings	Profile as per Figure 8
Top and Middle Ring (TMR)	Profile as per Figure 9
Load Balls	Φ95.25 mm – 116 numbers
Spacer Balls	Φ85.25 mm – 116 numbers
Lower race support Ring	A 300 mm thick rigid ring
Dead Load Ring attached to TMR	300 mm thick ring of 500 ton weight

b) Constraints Modeling

Different parts of the geometric model are constrained with respect to each other in order to achieve the desired motion of the components. Recurdyn supports various joint types such as fixed, rotational, cylindrical, spherical, translational, and Cartesian motion. Along with these joints it also supports constraints such as axis coincidence, in plane, on-off joint, etc,

Following joints are used in the large diameter bearing model.

i. Fixed joint between lower race and bearing support structure (ground) i.e., DOF =0.

ii. A joint between top race and bottom race with rotation about the bearing axis using Cartesian motion joint. Rotation is constrained at a specified angular velocity and all other degrees of freedom are left free. DOF =5.

iii. All the rolling elements are left free on the bearing raceways. So, each ball has 6 DOF. Balls will be constrained to move in the bearing race groove due to contacts modeled with top and bottom races.

c) Contact Modeling

In MBD simulations, contacts between parts are can be modeled only using pure penalty method. Modeling of contact in Recurdyn involves modeling of both contact stiffness and contact friction. The mathematical formulation used in MBD software is pure penalty method in order to reduce computational time. Recurdyn provides option to provide contact stiffness as value or as a load v/s penetration curve. Example of curve is provided in Figure 12.

Formulation is given below:

$$F = K\delta^n + C\left(\frac{d\delta}{dt}\right) \qquad \text{Eq. 3.1 [22]}$$

Friction force at the contact is modeled using static and dynamic threshold velocities as shown in Figure 11 in order to eliminate the discontinuity in friction coefficient modeling. Mathematical formulation of friction force is given in Eq. 3.2. Friction coefficient is modeled as shown in Figure 11. The friction coefficient value increases from zero to the static friction value as the relative velocity at contact increases from zero to static friction velocity (v_s). Then friction coefficient decreases to dynamic friction coefficient value as the slip velocity at the contact increases further to dynamic friction

velocity. After reaching dynamic friction coefficient value, it remains constant with any further increase in the slip velocity. Thus, the discontinuity in the friction coefficient value is eliminated.

$$F_f = \mu N \qquad \text{Eq. 3.2 [22]}$$

Contact parameters used in modeling ball to race, load ball to spacer ball and between TMR and top race are discussed in following sections.

i. Ball to Race Contact Modeling

Contact parameters to model bearing ball to race contact are calculated as per the Hertzian contact formulation described in the Ref. [1] and detailed calculation is shown in Ref. [23] .Contact formulation used in ball to race contact is presented below:

$$F = 2581637\ \delta^{1.5} + 2581.637\frac{d\delta}{dt} \qquad \text{Eq. 3.3 [23]}$$

Contact Stiffness (K) = 4.78×10^5 N/mm [Ref. 23]

Exponent (n) = 1.5

Damping Coefficient(C) = $\frac{K}{1000} = 480$ N.s/mm [Ref. 22]

Use of contact parameters from the Hertzian contact formulation restricts the contact penetrations to elastic deformations observed in ball to race contacts. As the contact penetration is equal to that of contact deformation, the effects of undulation profile on the dynamics of bearing ball movement in further models is simulated accurately as penetrations will not affect or reduce the effective undulation height (difference between the undulation height and contact penetration) in the bearing race. Moreover, by using Hertzian contact formulation in flexible multi body dynamic simulations helps in avoiding the need for fine mesh at the contact locations which is needed to capture the Hertzian contact deformations as the contact penetrations defined by Hertzian

contact formulation will account for these elastic deformations. So, these flexible bodies can be meshed appropriately to simulate just the bending of race thus reducing the computational intensity of the problem. Contact stiffness calculated by Hertzian formulation is provided as an input to the Recurdyn in the form of contact spline i.e., load vs. contact deformation curve as shown in Figure 12. Contact spline shows contact force against corresponding contact penetration or elastic deformation.

Other contact parameters such as damping coefficient, friction velocities are selected as per the best practices in MBD contact modeling mentioned in Recurdyn documentation [22]. Friction coefficients values for greased steel to steel surface contact are selected [26]. Contact modeling parameters between load balls and bearing race are shown below in Table 2.

Table 2: Contact Parameters of Load Ball to Race Contact

Contact Parameter	Value
K	2581637 N/mm
n	1.5
C	2581.637 N.s/mm
μ_s	0.24
μ_d	0.14
v_s	1 mm/s
v_d	2 mm/s

ii. Ball to Ball Contact Modeling

Spacer ball to load ball contact is also modeled as per sphere to sphere Hertzian Contact formulation [1]. Except for contact stiffness, exponent and damping

coefficient, all other contact parameters are same as that of ball to race contact presented in Table 2.

Contact Stiffness (K) = 4.78×10^5 N/mm [Ref. 23]

Exponent (n) = 1.5

Damping Coefficient(C) = $\frac{K}{1000} = 480$ N.s/mm [Ref. 22]

iii. Top and Middle Ring to Top Race Contact

The top and middle ring is in contact with top race by a flat surface to flat surface contact. Value of contact parameters are chosen as per best practices values provided in Ref. 22

Contact Stiffness (K) = 1×10^6 N/mm Ref. [22]

Exponent (n) = 2 Ref. [22]

Damping Coefficient(C) = $\frac{K}{1000} = 1000$ N.s/mm Ref. [22]

d) Loads and Boundary Conditions

Load and boundary conditions are to be defined on the model as the last step before solving for the results. Recurdyn provides for a number of different loads such as point load, pressure, gravitation load or self weight, moment, etc., and any of these loads can be applied on the model based on the requirement. Along with these, boundary conditions can be specified on the model such as initial position, initial velocity, and time based motions on any of the joints. These motions can be defined as a function time using various inbuilt functions.

In the bearing model, standard earth gravity is applied along the bearing axis in vertically downward direction as shown in Figure 12. Bearing top race surface is subjected to a symmetric load by the self weight of TMR. As the load is symmetric,

load is expected to be equally distributed among all the load balls. No motions are imposed on the bearing joints to perform static analysis and in case of dynamic analysis, rotational motion about the bearing axis is defined.

e) Solver

Recurdyn solver solves the equations of motion of all the bodies in the system. These equations are written in a matrix form as given in below in Eq. 3.4. This equation is rewritten in the form equation 3.5 which is solved by numerical integration with respect to time to obtain velocity and position of the bodies at every instant of time.

$$M(q)\frac{d^2(q)}{dt^2} + C\left(q, \frac{d(q)}{dt}, t\right) = Q(q, \frac{d(q)}{dt}, t) \qquad \text{Eq. 3.4 [22]}$$

$$\frac{d^2(q)}{dt^2} = M(q)^{-1}[Q(q, \frac{d(q)}{dt}, t) - C(q, \frac{d(q)}{dt}, t] \qquad \text{Eq. 3.5 [22]}$$

In Recurdyn, solver time steps are to be provided as an input. For the present bearing, dynamic analysis is performed with the default solver – Advanced Hybrid solver – with default settings of maximum time step equal to 1e-2 and initial time steps equal to 1e-6.

The solver automatically reduces the time step values depending on the solution convergence. In case of static simulations performed in next sections, a dynamic simulation is performed without rotation of the bearing until equilibrium is achieved i.e., damping off the initial vibrations caused in the system due to impact between the bodies under gravitational force. This equilibrium position is used as the initial position for the dynamic simulations performed by rotation of top race.

3.2 Validation of Static Analysis

A static simulation is performed on the bearing before performing dynamic analysis. At the end of static simulation system will reach equilibrium condition where all the bodies are at rest, balancing the gravitational force and loads acting on the system by developing reactions at the contacts and fixed joints modeled in the system.

Static simulation is performed by conducting a dynamic simulation without rotation of bearing. The bodies in the system under the action of gravitational force move due to close the initial gap between the bodies resulting in formation of contacts. During formation of contacts, bodies vibrate initially due the impact nature of contact formation which is damped off by the damping coefficient modeled in the contact. Conducting static simulation not only helps in checking the constraints and contacts in the system obtaining initial condition for dynamic analysis but also helps in. Moreover, loads acting on the bearing balls at the end of static simulations will give load distribution in the bearing under static condition. Validation of static simulation results on large diameter bearing is discussed below. Initially, a complete rigid body simulation is validated followed by flexible body simulation. In rigid body simulation all the bodies are modeled as rigid bodies that is structural deformation of bodies is not simulated. In case of flexible body simulation, top race and top and middle ring are simulated in order to simulate the effect of bending of bearing races under the influence of undulations

3.2.1 Validation of Rigid Multi Body Static Simulation

Static simulation is performed on the above described model for a sufficient period until all the body vibrations are died down, reaching equilibrium position, which is found to be around 5 seconds. This is pictorially shown in Figure 13.Forces experienced during static simulation by few selected bearing balls, which are selected from throughout the circumference is plotted in Figure 14 as a function of analysis time. It can be observed from Figure 14 that the initial vibrations of ball are completely died down by the end of static simulation, reaching equilibrium position.

It is observed that applied load is uniformly distributed on all the load balls. Normal contact force acting on each ball is found to be 49385 N. Static simulation results are validated against the analytical solution as shown below.

I. Analytical Solution

Load Applied on Top Race (A)	=	4905000N (500 ton)
Weight of Top race(B)	=	31817 N (3.25 ton)
Weight of Load Ball (C)	=	34.82 N (3.55 kg)
Number of Load Balls	=	116
Load per ball	=	$\frac{A+B}{116} + C$ = 42558.6 N

II. Static Simulation Solution

Normal Contact Force on Load Ball (D)	=	49385 N
Angle of Contact(e)	=	60°
Vertical Component of force on Load Ball	=	$D\ sin(e)$ = 42768 N
Error	=	0.5%

Static simulation results are found to be in agreement with analytical solution with an error of 0.5%. This error is within the acceptable limits. Thus, rigid multi body static simulation results are validated.

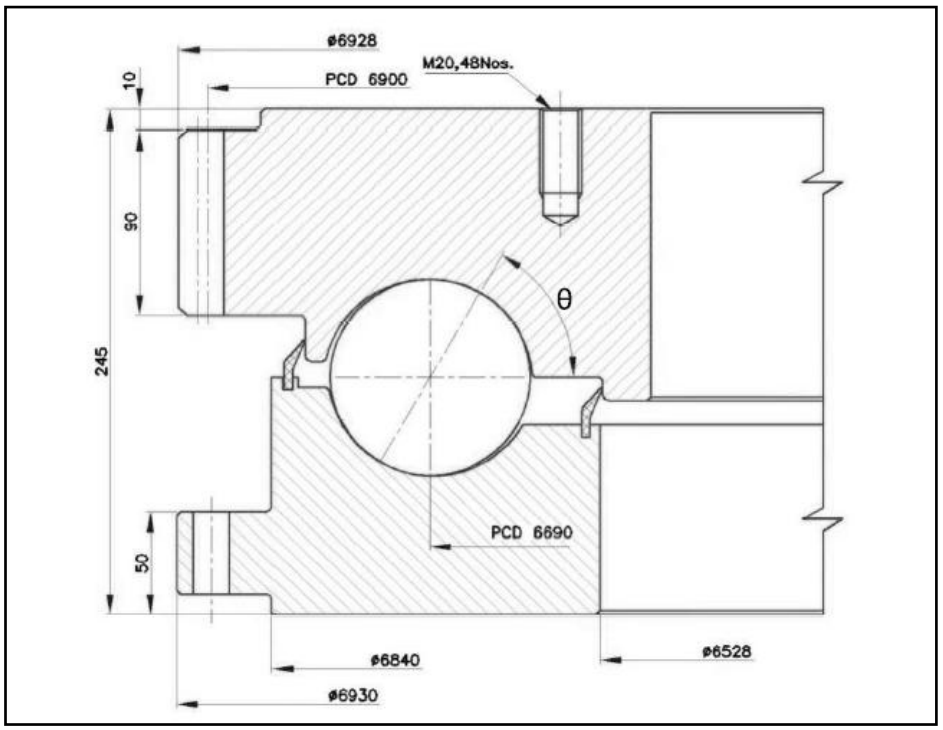

Figure 8: Cross Sectional View of Large Diameter Bearing Profile with Dimensions..

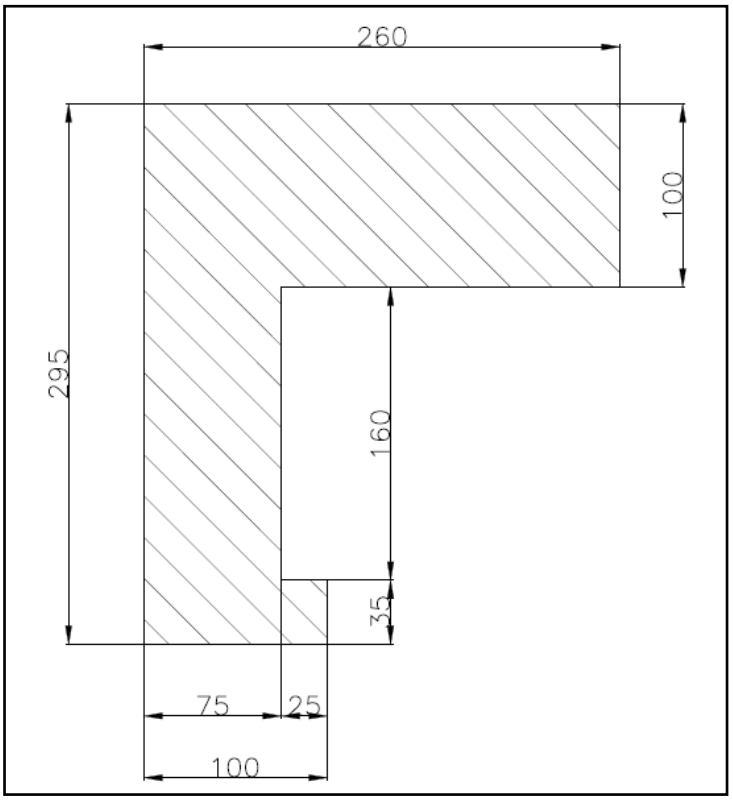

Figure 9: Cross sectional View of Top and Middle Ring (TMR).

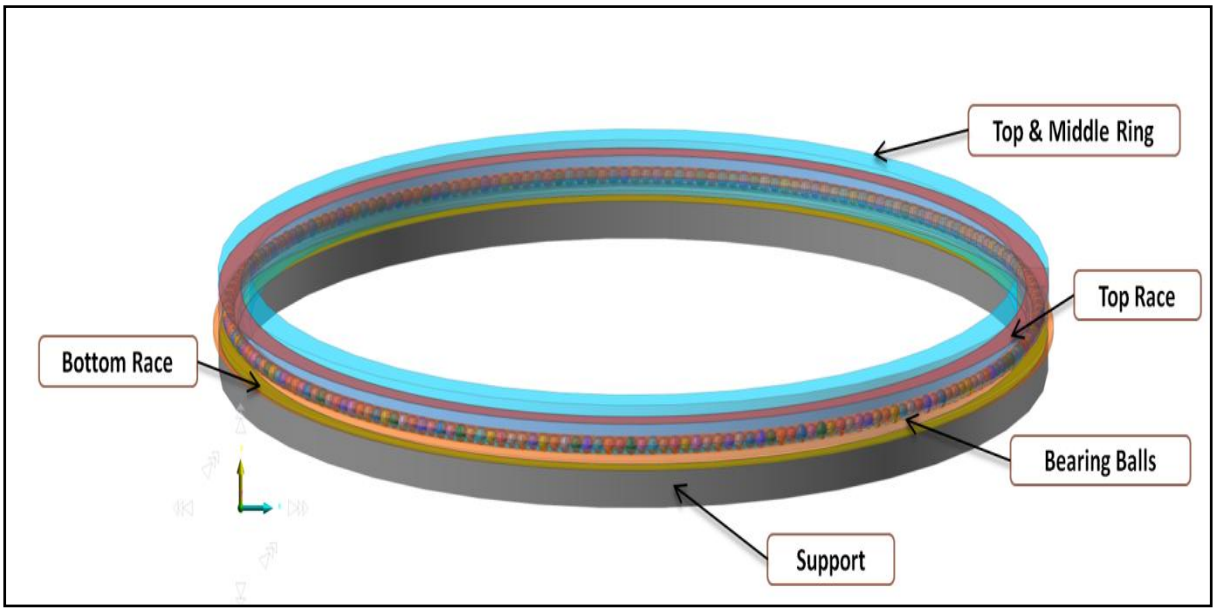

Figure 10: Geometric Model of Bearing

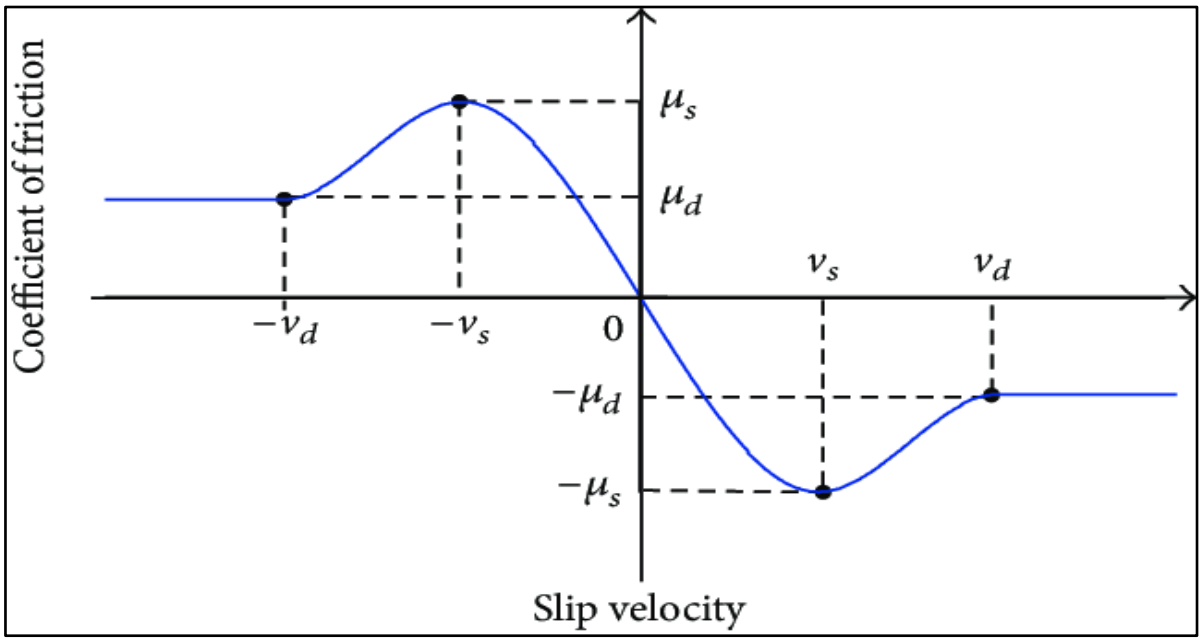

Figure 11: Friction Coefficient Modelling

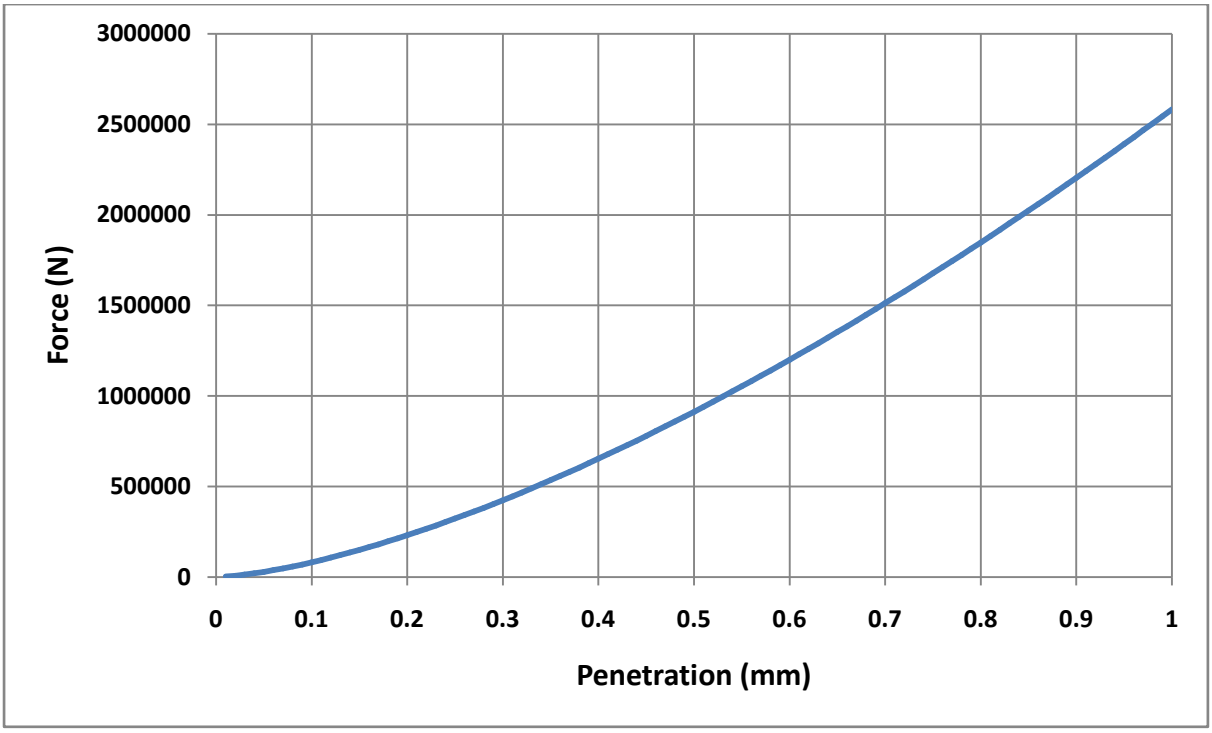

Figure 12: Contact Stiffness Spline for Ball to Race Contact

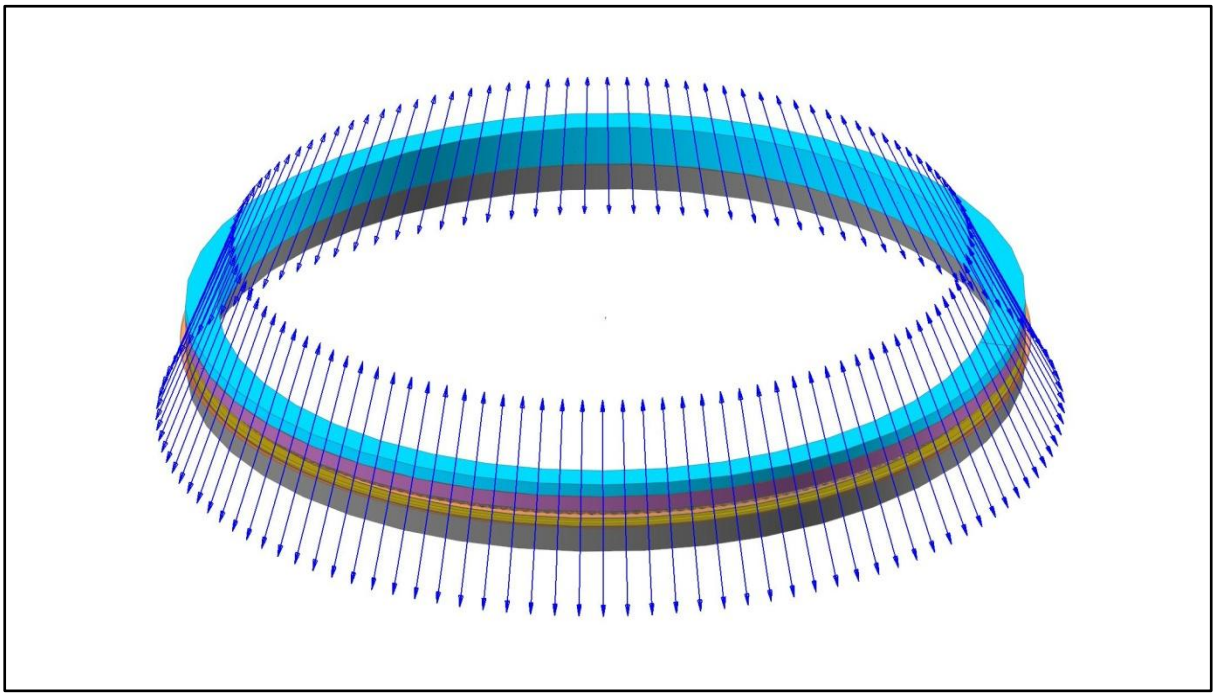

Figure 13: Load distribution in LRP bearing at the end of rigid body static simulation.

Blue arrows indicate force vectors

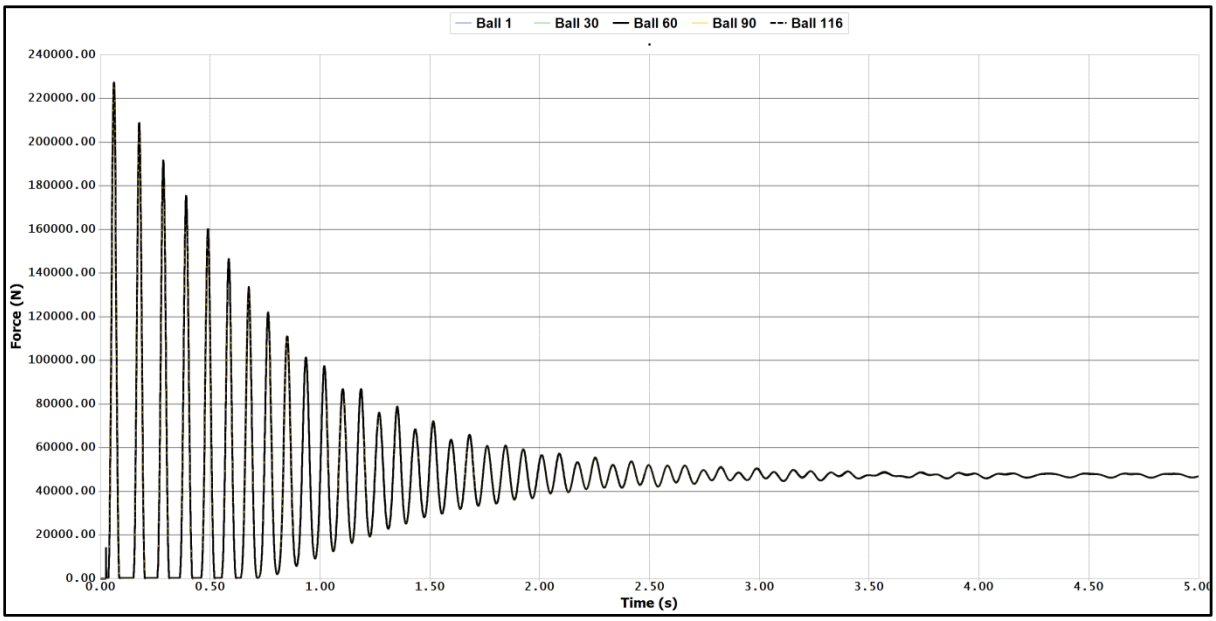

Figure 14: Rigid body static simulation results. Normal contact force on load ball is 49385 N.

3.2.2 Validation of Flexible Multi Body Static Simulation

In order to capture the bending behaviour of bearing race under the influence of undulations, top race and TMR are modelled as flexible bodies. As previously discussed in ball to race contact modelling, contact deformations are simulated by contact penetration without finely meshing the contact surfaces thereby reducing the computational time. So, the top race and TMR are meshed only to capture the bending of races under the influence of undulations.

Before employing the flexible multi body model to perform dynamic simulations, it is validated to perform static multi body simulation to obtain initial condition to start dynamic analysis. All the modelling details in flexible MBD simulation are same as rigid body simulation discussed in section 3.2.1. Meshing details of top race and TMR are shown in Table 3.

Table 3: Top Race and TMR Meshing Details

Parameter	Top Race Meshing Details	TMR Meshing Details
Element Type	Eight and Six Node Solid Element	Eight Node Solid Element
No. of Elements	36000 Solid8: 35250, Solid6: 750	26500
No. of Nodes	48750	34000
Mesh Quality	Maximum Aspect Ratio is 2. Dominant Aspect ratio is in between 1 to 1.5.	Maximum Aspect Ratio is 2. Dominant Aspect ratio is in between 1 to 1.5

As done in previous case, static simulation is performed for a period of 5 seconds until all the body vibrations are died down reaching equilibrium position. This is pictorially shown in Figure 15. Force experienced by bearing balls during static simulation is shown in Figure 16. It can be observed from Figure 16 that the initial vibrations of balls are completely died down by the end of static simulation, reaching equilibrium position.

It is observed that applied load is uniformly distributed on all the load balls. Normal contact force acting on each ball is found to be 49385 N.

Static Simulation Solution

Normal Contact Force on Load Ball (D) = 51103 N

Angle of Contact(e) = 60°

Vertical Component of force on Load Ball = $D\ sin(e)$ = 44246.5 N

Error = 4%

Static simulation results are found to be in agreement with analytical solution (discussed in 3.2.1 with an error of 4%.Thus flexible multi body static simulation results are validated.

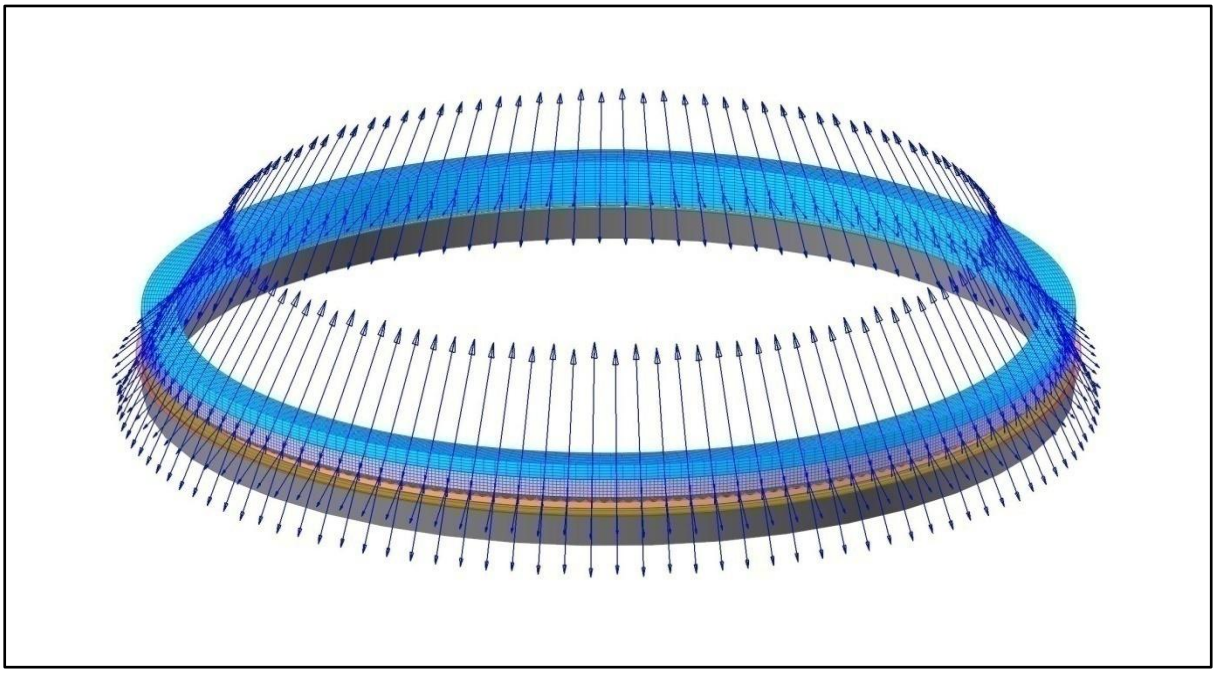

Figure 15: Load distribution in LRP bearing at the end of flexible body static simulation - Blue arrows indicate force vectors

3.3 Validation of Dynamic Analysis

Prior to performing dynamic simulations, Recurdyn dynamics solver is validated to perform dynamic simulations on ball bearing. Initially, an attempt was made to perform validation on a ϕ6.9 m bearing (full scale) model, but due to long computational time taken, a scale down model of one meter diameter with all other geometric features remaining same is used. Reasons for long computational time in full scale bearing dynamic simulation are

1. Large number of nodes and elements present in the full scale model.
2. As the number of balls are high (232 balls –spacer and load balls) in a full scale model, the number of contacts to be simulated is also high (696 contacts).

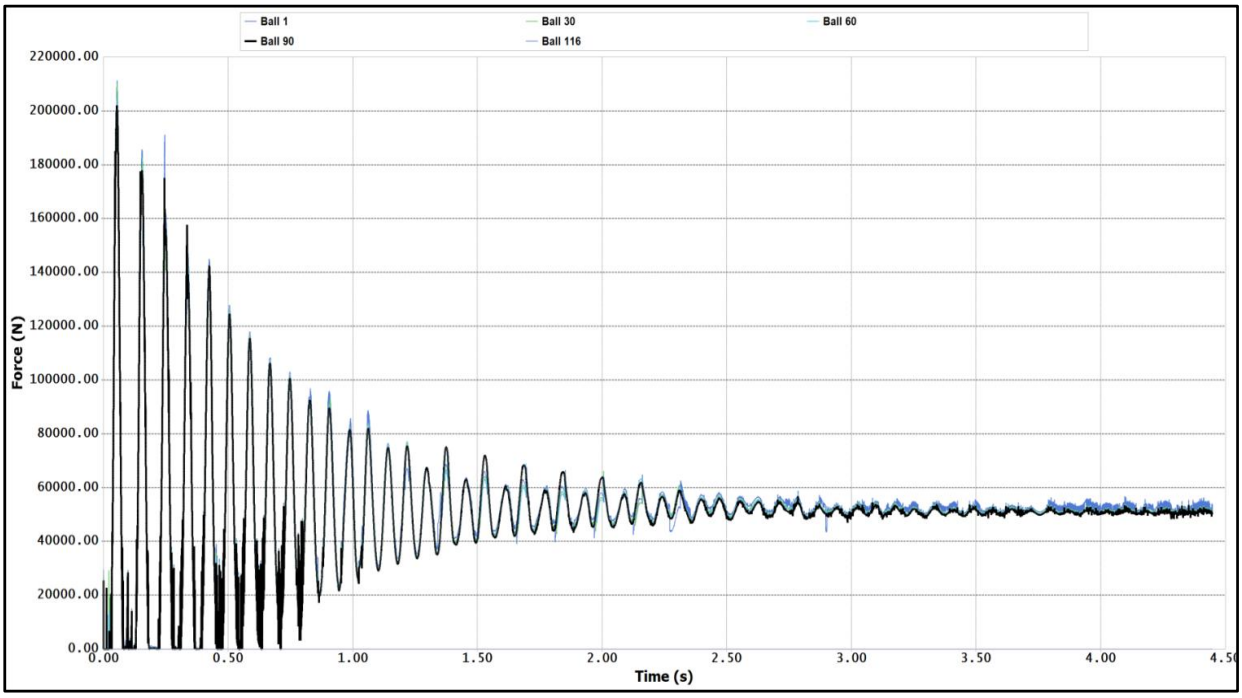

Figure 16: Flexible body static simulation results. Normal contact force on load ball is 51103 N

3.3.1 Geometric Details of Scaled Down Model of Bearing

Geometric model of scaled down bearing model (ϕ 1 m) is shown in Figure 17. Geometric details are mentioned below.

Pitch diameter of bearing	=	1000 mm
Diameter of load ball	=	95.25 mm
Diameter of Spacer ball	=	92 mm
Number of load and spacer ball pairs	=	16

3.3.2 Load Applied on Scaled Down Bearing Model

To validate the dynamic analysis, axial thrust load is applied on the bearing to obtain equal load distribution on all the balls as in the case off static simulation validation.

Load per load ball in full scale bearing	=	4.31 ton

For 16 number of load balls in scaled down model equivalent load = 68.9 ton

3.3.3 Constraints and Contact Modeling in Scaled Down Bearing

Constraints in the model are same as full scale model with rotational joint modelled to rotate top race. Rotational speed of top race is modified to reduce the computational time to obtain results for one complete rotation of bearing balls to reduce computation time. Details of bearing rotation are discussed below.

- Max. Angular velocity of full scale LRP bearing = 0.196 rpm.
- In order for bearing balls in scaled down model to have same linear velocity as that of the balls in full scale LRP bearing, required angular velocity is 1.311 rpm. One complete rotation of the bearing race with above speed requires 45 seconds (which required 14 days of computational time for flexible analysis)
- So, the rotation speed of bearing is increased by 5 times in order to obtain the two rotations (one rotation of ball) within18seconds simulation time, which corresponds to 8 days of computational time.
- Assigned angular velocity to scaled down model = 6.55 rpm

Contacts in the bearing are modelled as per the details given in Section 3.1.

3.3.4 Validation of Rigid Multi Body Dynamic Simulation

The dynamic simulation is performed on the scaled down bearing model for a period of 25 seconds, with an initial static simulation running for 3 seconds until all the body vibrations are died down reaching equilibrium position. Following the static simulation, the top race is rotated for 22 seconds with a speed of 6.55rpm as discussed above.

Force experienced by bearing balls during dynamic simulation is shown in Figure 18and Figure 19. It can be observed from the Figure 19 that loads are equally distributed on the bearings.

- **Analytical Solution**

Load Applied on Top Race (A)	=	675909 N (68.9 ton)
Weight of Top race(B)	=	4767.66 N (0.486 ton)
Weight of Load Ball (C)	=	34.82 N (3.55 kg)
Number of Load Balls	=	16 (8 Load + 8 Spacer Balls)
Load per ball	=	$\frac{A+B}{16} + C$ = 42577 N

- **Dynamic Simulation Solution**

Normal Contact Force on Load Ball (D)	=	47226 N
Angle of Contact(e)	=	60°
Vertical Component of force on Load Ball	=	$D\ sin(e)$ = 40990 N
Error	=	3.64%

Dynamic simulation results are found to be in agreement with analytical solution within an error of 3.64%. This error is within the acceptable limits. Thus, rigid multi body dynamic simulation results are validated.

Similarly, dynamic simulation is conducted with flexible top race and TMR and is explained in following Section.

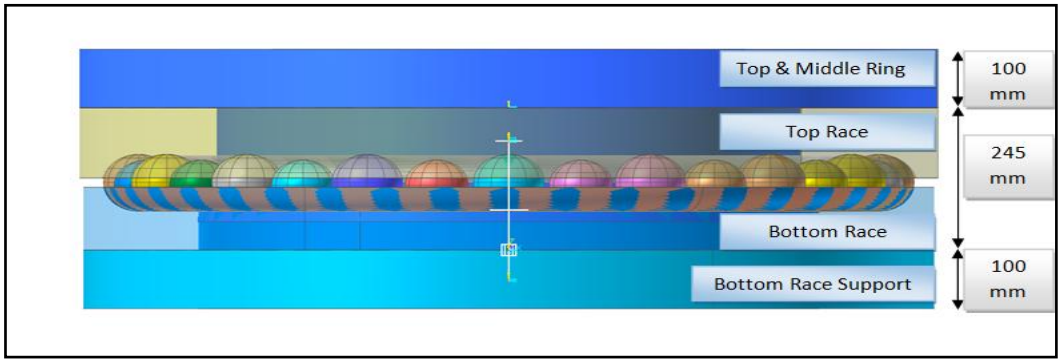

Figure 17: Geometric Model of Scaled Down One Meter Diameter LRP Bearing

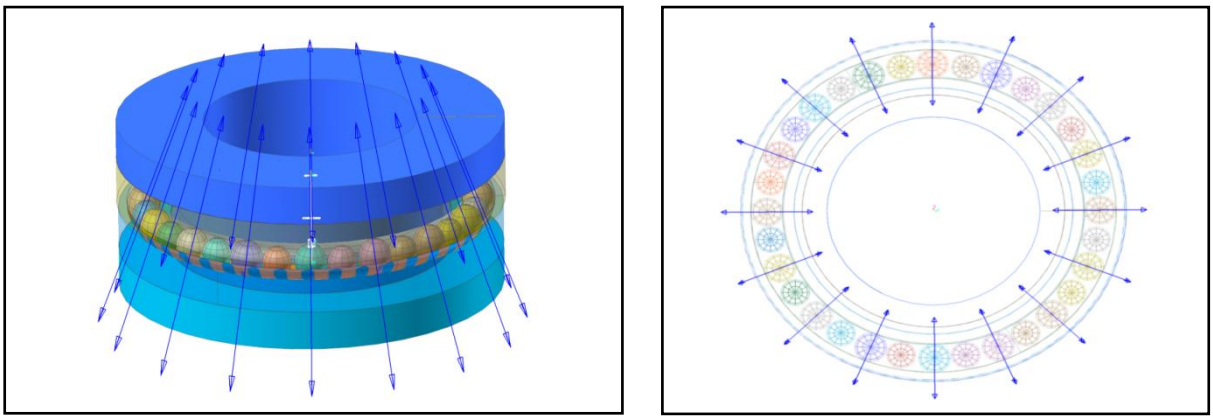

18.1 Front View **18.2 Top View**

Figure 18: Load Distribution on Bearing Balls during Top Race Rotation

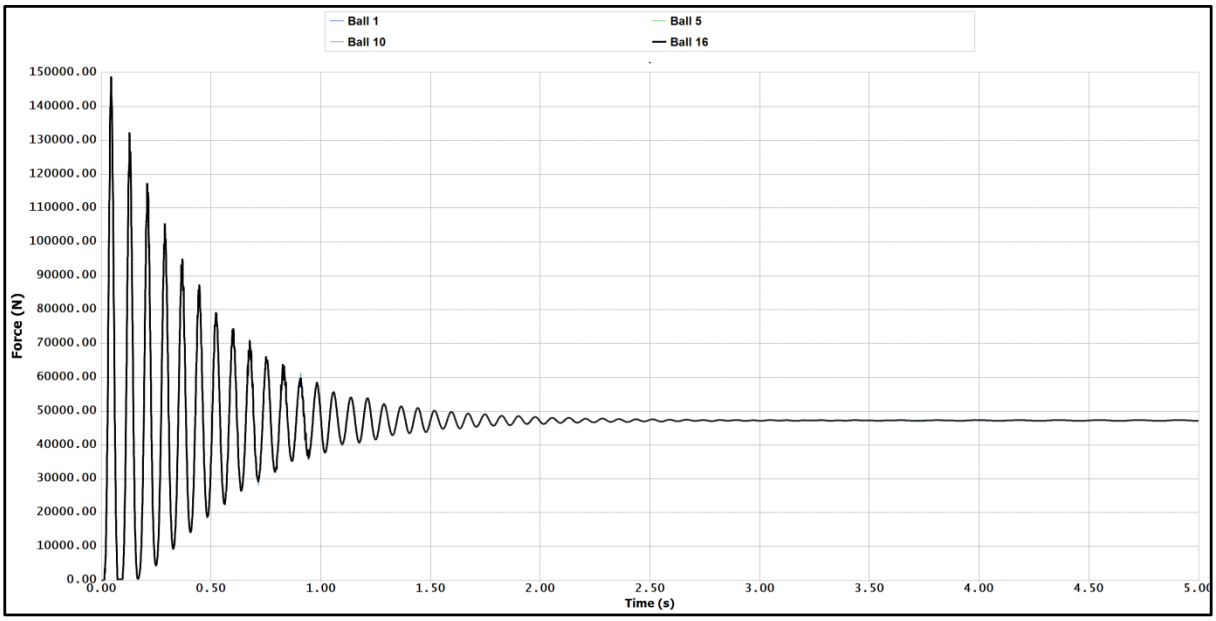

Figure 19: Rigid Multi Body Dynamic Simulation Results

3.4 Validation of Flexible Multi Body Dynamic Simulation

A dynamic simulation is performed on the scaled down bearing model with flexible top race and TMR. The top and bottom races are modeled as flexible bodies by meshing the geometric models using FEA based flexible body solver.

Simulation details are same as that of rigid body simulation as discussed in 3.3.4. Flexible body meshing data is presented in Table 4.

Table 4: Meshing Data of Scaled Down One Meter Diameter Bearing

Parameter	Top Race	Top and Middle Ring
No. of Nodes	9603	10961
No. of Elements	7051	8561
Element Type	Solid 8 (Hexa 8) 8 nodes	Solid 8 (Hexa 8) 8 nodes
Mesh Quality: Aspect Ratio	1 to 1.2 (acceptable)	1 to 1.2 (acceptable)

Force experienced by bearing balls during dynamic simulation is shown in Figure 20and Figure 21. It can be observed from the Figure 21 that loads are equally distributed among the bearing balls.

- **Flexible Body Dynamic Simulation Solution**

Normal Contact Force on Load Ball (D) = 50471 N

Angle of Contact(e) = 60°

Vertical Component of force on Load Ball = $D\ sin(e)$ = 43704 N

Error = 2.7%

Static simulation results are found to be in agreement with analytical solution within an error of 2.7%. This error is within the acceptable limits. Thus, flexible multi body dynamic simulation results are validated.

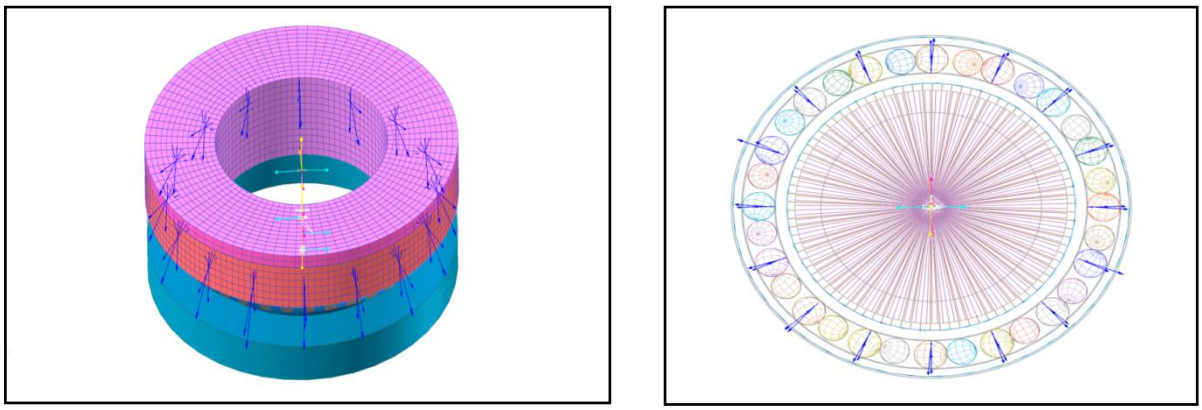

20.1 Front View **20.2 Top View**

Figure 20: Load Distribution on Bearing Balls during Top Race Rotation in Flexible Multi Body Simulation

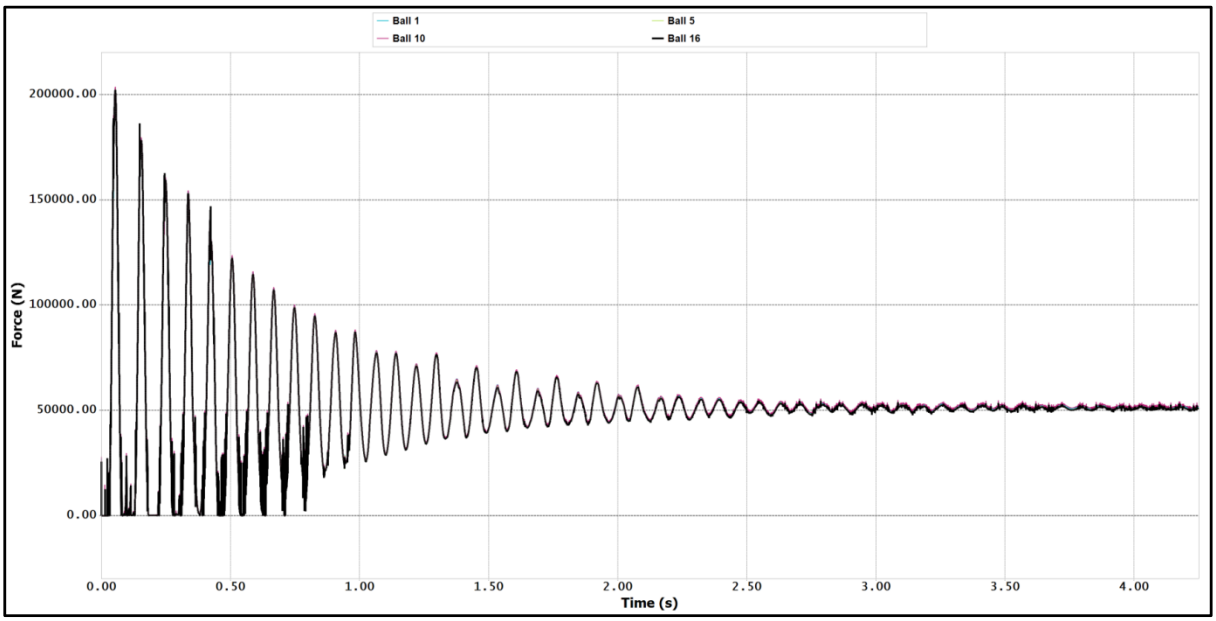

Figure 21: Flexible Multi Body Dynamic Simulation Results

3.5 Comparison of Finite Element Method (FEM) based and Component Modal Synthesis (CMS) based Flexibility Modeling of Bodies

Validation of dynamic analysis is performed in Section 3.3 and 3.4. But the computational time taken for 25 seconds of simulation time on a scaled sown model is 8 days

on Intel Xenon processor with 128GB RAM. In order to further reduce the computational time and to model larger size bearing, various options are considered and use of component modal synthesis (CMS) based flexible body simulation in place of FEA based simulation (which is used in section 3.4) is considered to be one possible option. In Recurdyn tool, FEA based flexible modeling is referred as Full Flexibility model and CMS based model as Reduced flexibility model.

In FEA based modeling, deformation of body is computed using finite element method. In case of component modal synthesis (CMS) model [27], deformation of body is calculated by using mode shapes of the body under the applied constraints. As bending deformation calculation is important from the point of view of simulating influence of undulations, bending behavior of top race is compared when modeled using CMS and FEA method. To validate the results, bending behaviour of top race using MBD models (that is both CMS and FEA based flexibility models are compared with FEA based beam model. The models used are assigned same cross section and material properties as that of top race. The details of these analyses are described in following sections. Difference between these two modelling techniques is presented in Table 5.

Table 5: Comparison of Flexibility Models

S. No	Full Flexibility (FEA)	Reduced Flexibility (CMS)
1	Non- linear material can be used.	Limited to linear material.
2	Large deformations can be simulated.	Limited to small deformations.

3	External loading points and joint positions can be changed during simulation. Contact points can change.	External load points and joint positions cannot be changed during simulation as the mode shapes used for the simulation are calculated using the initial load points and joints. Contact points can change.
4	Computational time is high.	Computational time is low.

3.5.1 Validation of FEA Based Beam Model

Prior to taking-up FEA based beam analysis for top race in Recurdyn, a simple curved beam analysis for a circular cross section beam was carried out and the results are compared with the analytical solution.. Beam is modelled as a 180° sector of circular cross section with Beam 188 elements capable of simulating Euler-Bernoulli beams. Load is applied on the beam as uniformly distributed load (UDL) with both ends fixed.

I. Model Details

Load (P) = 20kN

Radius (R) = 500mm

Radius of cross section (r) = 60mm

Young's Modulus (E) = 200GPa

Passion's Ratio = 0.3

II Analytical Solution [24]

Following equation is used for calculating the midpoint deflection

$$\text{Maximum Deflection} = 0.25828\left(\frac{PR^3}{EI}\right) = 5.337 \text{ mm}$$

III FEA Simulation

The deflection behavior of the beam is shown Figure 22. Based on the FE analysis, the maximum deflection is found to be 5.3 mm with an error of 0.7%. Error is within acceptable limits. This beam analysis is used to validate MBD model's bending capabilities. Deflection of beam is shown in Figure 22.

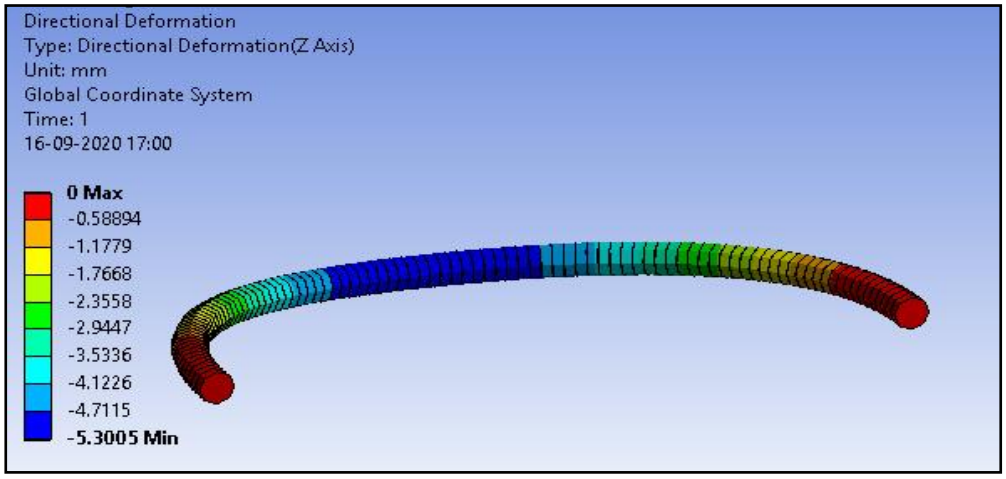

Figure 22: Deflection Plot of Beam using FE-Beam Model Analysis (Maximum Deflection is 5.3 mm)

3.5.2 Comparison of Bending Deflection in Reduced and Full Flex Models

After validating the beam analysis capabilities in Recurdyn, comparison of bending behaviour of top race using reduced and full flexibility is taken-up in Recurdyn as a step towards validating the use of flexibility analysis for further simulations to study effects of undulations on bearing. The results are compared with the FE based beam analysis for validation. Model details are discussed below. Load applied is equal to the pressure loading on the LRP bearing.

I. Model Details

Load (P)	=	218.6 N/mm
Radius (R)	=	500mm
Cross section (r)	=	Top Race cross section (Figure 8)

Young's Modulus (E) = 200GPa

Possion's Ratio = 0.3

II. FEA Simulation Result

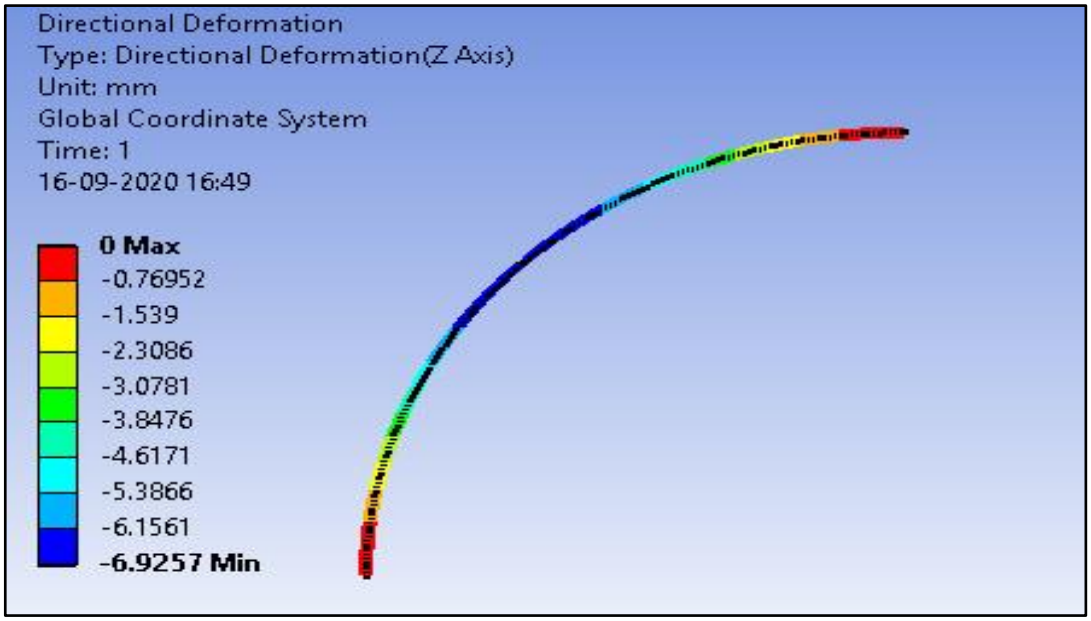

Figure 23: Beam FEA Model Deflection of Top Race. Maximum Deflection is 6.92 mm

III. Full Flex Simulation Result

A static simulation is performed for a sufficient period of time to obtain deformation of FEA based full flex top race under the pressure load defined above. The deflection is calculated by resting the top race on only four balls fixed at 90° apart in the bearing.

The Maximum Deflection is found to be 6.49 mm.

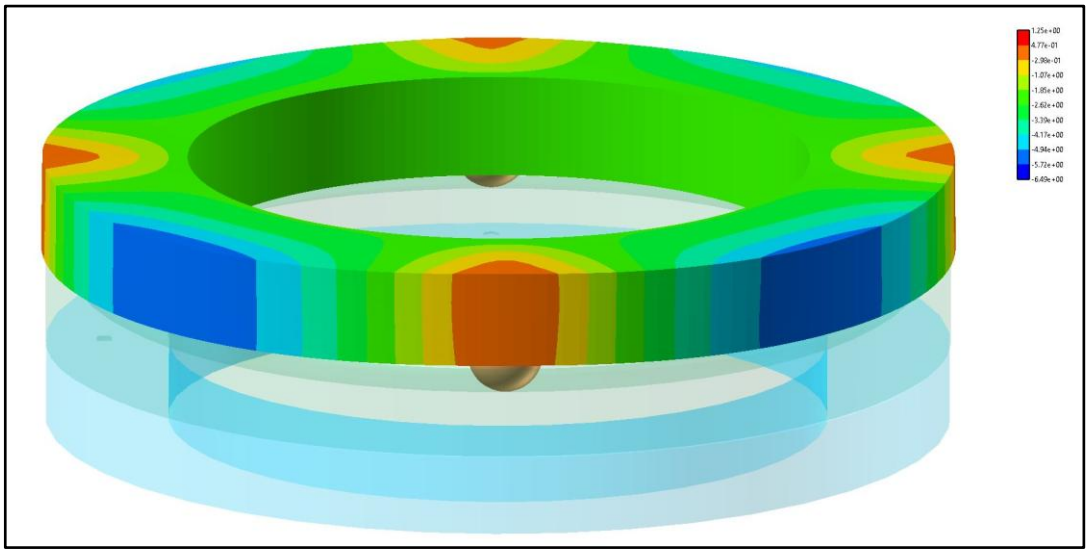

Figure 24: Beam FEA Model Deflection of Top Race. Maximum Deflection is 6.49 mm

IV. Reduced Flex Simulation Result

A static simulation is performed for a sufficient period to obtain deformation of CMS based reduced flex top race under the pressure load and boundary conditions defined above. Maximum Deflection is found to be 6.47 mm.

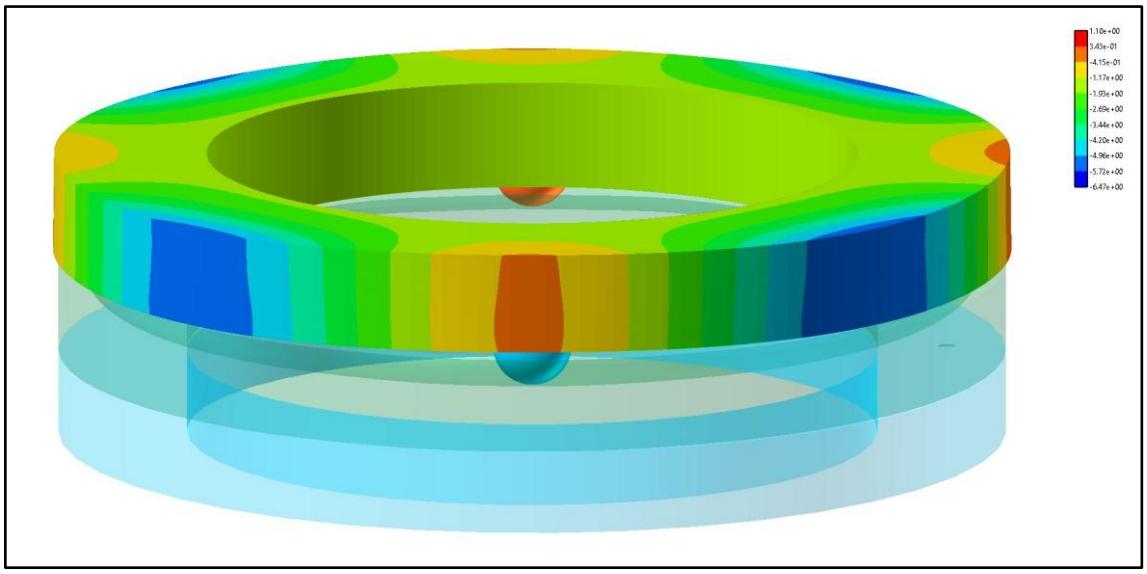

Figure 25: Beam FEA Model Deflection of Top Race. Maximum Deflection is 6.47 mm

From above results, it can be seen that MBD results are in close agreement with beam FEA model validating the deformation behavior in MBD flexible bodies. Moreover, both

full flex and reduced flex bodies show similar deformation behavior. Thus CMS based or reduced flexible model is validated for studying the influence of undulation, which significantly brings down the computation time and thereby facilitates longer analysis time.

3.5.3 Validation of Flexible MBD model on Undulated Profile

In the above sections, MBD solver is validated to be used in static dynamic simulations without undulations. Furthermore, bending behaviour of flexible bodies is also validated. As static simulation results are validated completely, validation of dynamic simulation results at a given instance of time (or rotational position of top race) by comparing with static simulation results for the same rotational positions of all bodies at that given instance will further improve confidence in dynamic analysis results.

To perform this validation, bearing with undulations geometrically modelled in the bottom race as per the undulation profile as shown in Figure 6 is rotated by 180°. Load distribution in the bearing at the end of simulation is extracted. Positions of all bodies at the end of dynamic simulation (i.e., top race rotated by 180°) are extracted to perform a static simulation. Load distribution in static and dynamic simulations is compared to validate the solver.

With the use of reduced flexible model or CMS based flexibility model we can afford to simulate lager sized bearings as the constraints on computational time are relaxed. Thus a bearing model with pitch diameter of 2 meters is used in further study. In this model increased spacer ball diameter of Φ92 mm is used instead of Φ85.25 mm used in one meter bearings in order to use the spacer balls of same dimension as that are proposed for large diameter bearing. Load on the bearing is also proportionally increased with respect to number of load balls.

I. Model Details

Pitch Diameter of Bearing	=	2 m
Diameter of Load Ball	=	95.25 mm
Diameter of Spacer Ball	=	92 mm
Number Load Ball and Spacer Ball Pares	=	33
Load on Bearing	=	140 ton
Constraints and contact modeling	=	Same as that of one meter bearing
Rotation speed of Top Race	=	6.55 rpm
Extent of Rotation in Dynamic Simulation	=	180°
Young's Modulus	=	200 GPa
Poisson's Ratio	=	0.3

II. Results

Dynamic and static simulations as per the methodology discussed above are performed to obtain load distribution in the bearing. Along with these simulations, static simulation is also performed at initial condition, results of which are presented in Figure 26 along with other results.

From the results (Figure 26) showing dynamic and static MBD analysis results at top race rotation of 180º, following observations are made.

1. Load distribution in static and dynamic analyses is roughly alike in trend.
2. There is considerable variation in the load distributions at the locations before and after zero load zones as shown in the graph.
3. Load balls entering the zero load zones in dynamic simulation experienced less load and load ball leaving the zero load zone experienced high load when compared to static simulation results.

4. The above variations can be attributed to the inertia effects present in dynamic simulation due to the movement of the balls. As the bearing balls are in motion in dynamic analysis they move into zero load zone with ease as it involves relaxation of contact deformation formed at its contact with bearing races and moving out of zero load zone needs extra effort as the contact are to be deformed on its entry into contact with top race of the bearing. In case of static analysis, ball are in static condition and hence, there is no movement of balls into or out of zero load zones rendering them to maintain their contacts constantly throughout the simulation. Thus, the dynamic analysis results show low load at the entry of zero load zone and high load at the exit of zero load zone when compared to static simulation.

From the observations stated above, Recurdyn-a general purpose multi body dynamics solver- is demonstrated to perform dynamic simulations with undulations.

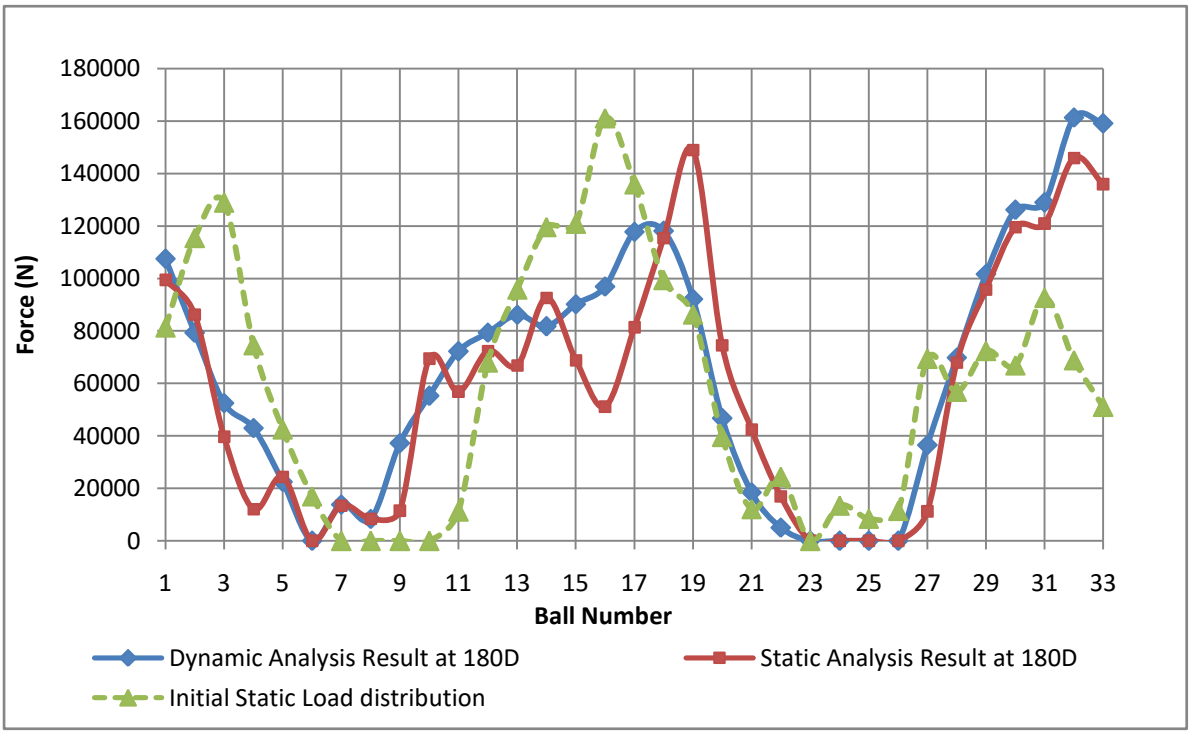

Figure 26: Load Distribution in Bearing under the Influence of Undulations after 180° Rotation of Top Race

3.5.4 Equating Bending Stiffness of Full Scale Bearing Top Race and TMR to that of Two Meter Bearing

As reduced flexibility model (CMS model) has same bending behaviour as that of full flexible model (FE based model), it is used in further dynamic simulations of two meters diameter bearing at the same computational cost of one meter full flex model (8 days). Further, in order to obtain or ascribe same bending behaviour of full scale bearing (ϕ6.69 m) in two meter bearing to study undulation effects, flexural rigidity of two meter bearing is reduced to that of ϕ6.69 m bearing by reducing Young's modulus of the top race and TMR material. This calculation with validation using FEA solver (ANSYS Mechanical) is discussed below.

Deflection of Beam under uniformly distributed load $\alpha \quad \frac{wl^4}{EI}$ Eq. 3.4

Bending Stiffness $\alpha \quad \frac{l^4}{EI}$ Eq. 3.5

Where,

w = Line pressure

l = length of beam

E = Young's Modulus (E_1= 200GPa for 6.69 m bearing, E_2 for 2 m bearing)

I =Areal Moment of Inertia

In order to have same bending stiffness as that of ϕ6.69 meter bearing in ϕ2 meter bearing, Young's modulus of ϕ2 meter bearing is adjusted as below.

$$E_2 = E_1 (2/6.69)^4$$

$$E_2 = 1.5975 \text{ GPa}$$

Validation of calculated E_2 is performed by comparing the deflection of Φ6.69 meter bearing and Φ2 meter bearing with Young's modulus E_1 and E_2respectively. To perform

this validation, top race is modelled as 90° sector with both ends fixed as shown in Figure 25. Line pressure of 218.5 N/mm is applied on the race. Deflections of full scale and scaled down models are shown in Figure 27 and Figure 28. As deflection of reduced stiffness model of Φ2 m bearing is in agreement with that of full scale bearing, bending behaviour of full scale bearing is simulated with two meter scaled down bearing. Thus, the effect of undulations on load distributions in scaled down model will be same as that in full scale model.

3.6 Summary

A large diameter bearing is modelled in a general purpose multi body dynamics tool to demonstrate the tool to study influence of undulation in the bearing. A detailed discussion is presented on modelling large diameter bearing with constraints and parameters used in contact modelling. Initially, static simulation results are validated on full scale bearing model of ϕ6.69 m using both rigid and flexible body analysis. Then, due to computational constraints in dynamic analysis, a scaled down model is used to validate the Recurdyn dynamic solver. In order to reduce the computational time, component modal synthesis (CMS) method of creating flexible bodies is explored and validated its use in the study. Using this method with increased size of the bearing, a dynamic analysis is performed with undulations modelled in the bearing to demonstrate the use of multi-body dynamic simulations in studying the influence of undulation on load distribution in the bearing.

Further, reduced stiffness model of two meter diameter bearing is modelled to ascribe same bending stiffness as that of full scale model by reducing the flexural rigidity. This model reduces the computational time by simulating bending behaviour of full scale model in a scaled down model. This model is further used in the next chapters to study of effects of undulations on load distribution.

Table 6: Deflection of Inherent and Reduced Stiffness Models

Deflection in full scale bearing model with inherent stiffness	115 mm
Deflection in scaled down model with inherent stiffness	0.96 mm
Deflection in scaled down model with reduced stiffness	117.3 mm

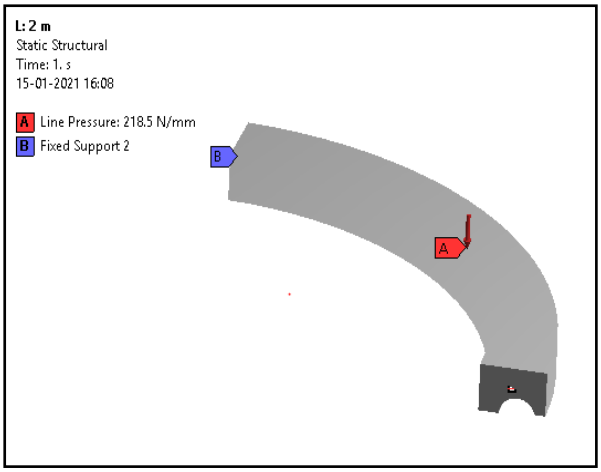

Figure 27:Geometric Model

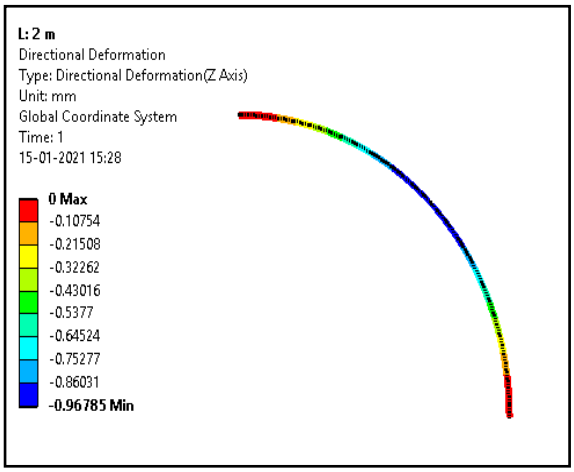

Figure 28: Deflection of Φ2 m bearing-Inherent Stiffness

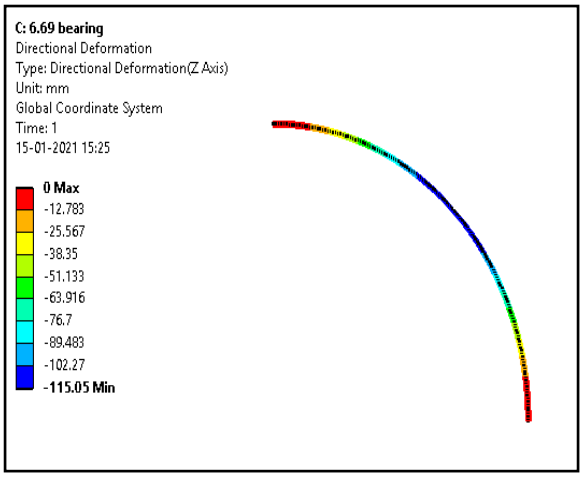

Figure 29:Top Race Deflection of Φ6.69 m Bearing

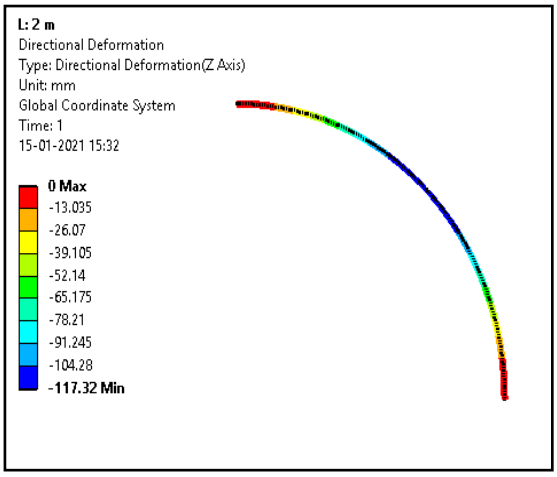

Figure 30:Top Race Deflection of Φ2 m bearing with reduced stiffness

CHAPTER 4

RESULTS AND DISCUSSION ON INFLUENCE OF UNDULATIONS ON LOAD DISTRIBUTION IN BEARING

Presence of undulations in the bearing adversely affects the load distribution in the bearing causing few balls to experience very heavy loads during bearing operation. This results in decreased bearing fatigue life. In order to estimate load distribution in the bearing under the influence of undulations, multi body dynamics simulations are performed using the bearing models discussed in sections 3.5.4 and 3.5.5. Following load cases are simulated in this study.

1. Effects of undulations formed due to elastic deformation of support structure, manufacturing defects etc., on the load distribution in two meter scaled down model. A parametric study is also conducted by varying the height of undulations.
2. Effects of Differential thermal expansion formed due to non-uniform temperature gradient along the bearing circumference on the load distribution in two meter scaled down model.
3. Combined effect of undulations and differential thermal expansion.

4.1 Effect of Undulations on Load Distribution in Bearing

Following simulations are performed to study the effects of undulations on bearing performance.

1. MBD simulation with undulation profile (as shown in Figure 6) geometrically modeled in bottom race, TMR and top race modeled with inherent stiffness i.e., Young's modulus is 200GPa (see Section 3.34).
2. MBD simulation with undulation profile (as shown in Figure 6) geometrically modeled in bottom race, TMR and top race modeled with reduced stiffness i.e.,

Young's modulus is 1.5975GPa (see Section 3.34) to simulate the stiffness of full size diameter bearing.

3. A parametric study is conducted to study the effect of undulation height on load distribution in the bearing.

4.1.1 Bearing Load Distribution under the Influence of Undulation Profile

A two meter diameter bearing having same cross section as that of large size bearing as described in Chapter 3 with top race and TMR modeled with inherent and reduced bending stiffness are used to study the effects of undulations. Undulations are geometrically modeled in the bottom race as per the undulation profile shown in Figure 6. Simulation is performed to rotate bearing top race by two rotations in order to complete one full rotation of bearing balls. Results are presented below along with load ball to spacer ball interaction force.

Following are the observations from load distributions as presented in Figures 31,32and 33.

1. Load distribution is found to be in agreement with the undulation profile i.e., bearing balls located on undulation high points experienced high load compared those in the other locations. Moreover, balls present in the low points in undulation valley experienced zero loads due to loss of contact with top race.
2. Maximum load in a bearing ball with top and bottom races modeled with inherent stiffness is high when compared to that of reduced stiffness model. Maximum load in inherent stiffness model is 16.7 ton whereas maximum load in reduced stiffness model is 12 ton; this difference can be attributed to better bending behavior of reduced bending stiffness model leading to more number of balls coming in contact in-between bearing races resulting uniform load distribution.

3. Total number of load balls which lost contact with top race is 7 in both the models. Loss of contact is due to inability of bearing race to bend and make contact with load balls at the low points in undulation profile.
4. From Figure 33, it can be observed that a peak contact force between the load and spacer ball is 625 N.
5. The peak contact force between the load and spacer ball occurs prior to the ball move to peak undulation height. From this, it can be inferred that the load ball is being pushed by the spacer ball to climb the peak undulation height.

Above observations suggest a significant influence of undulations on the load distribution. To further study the effect of undulation height, a parametric study is conducted.

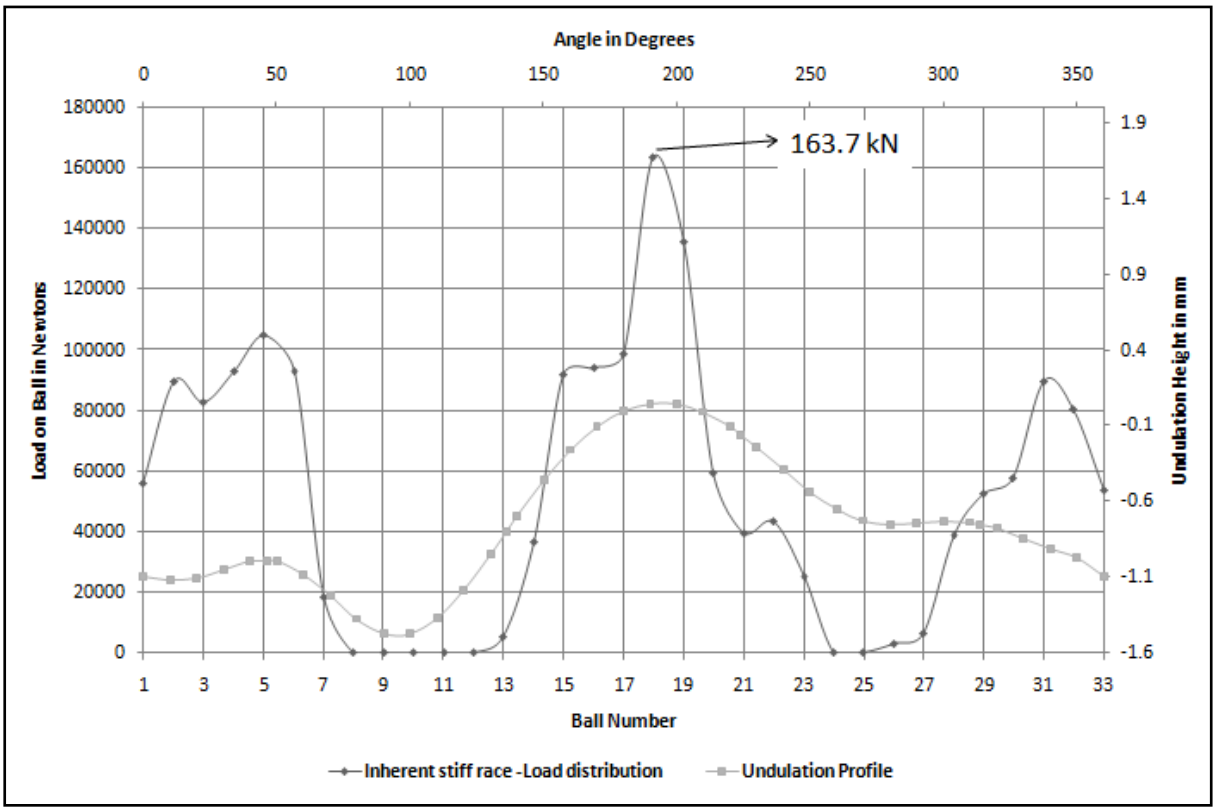

Figure 31: Load Distribution under the Influence of Undulation - Inherent Stiffness Model, Maximum load is 163.7 kN

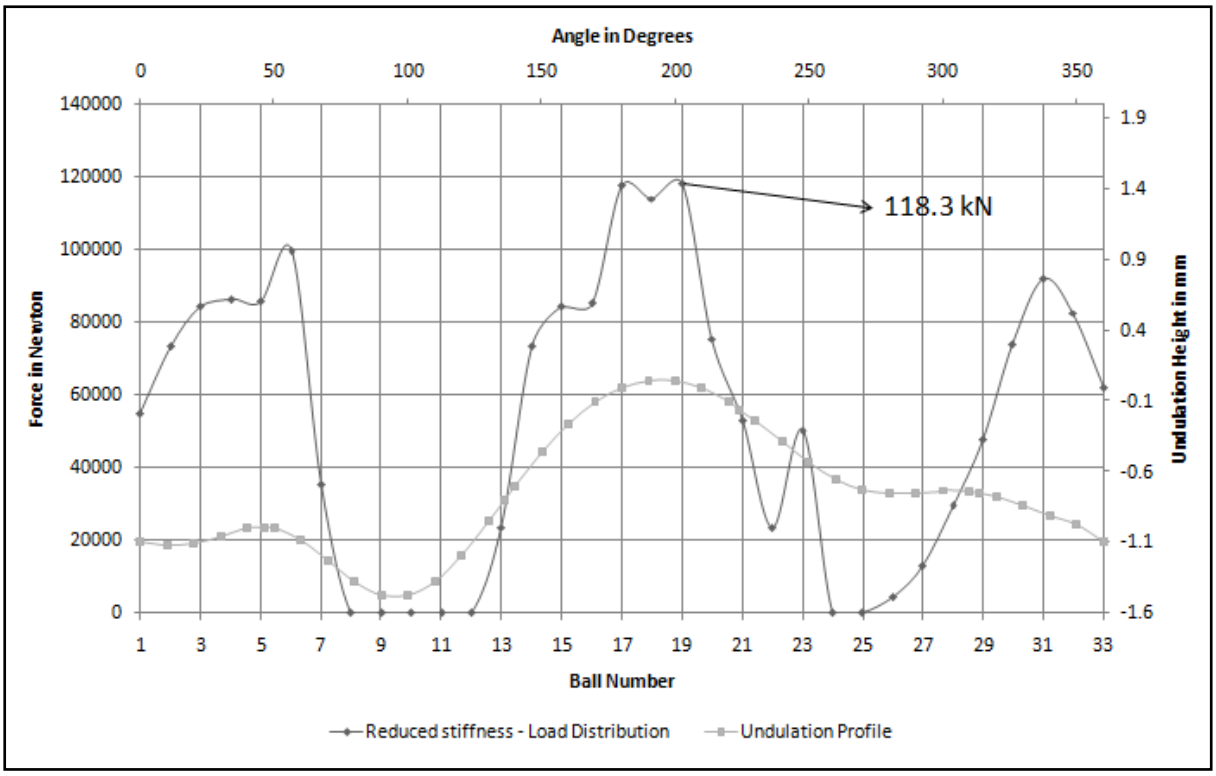

Figure 32: Load Distribution under the Influence of Undulation - Reduced Stiffness Model, Maximum load is 118.3 kN

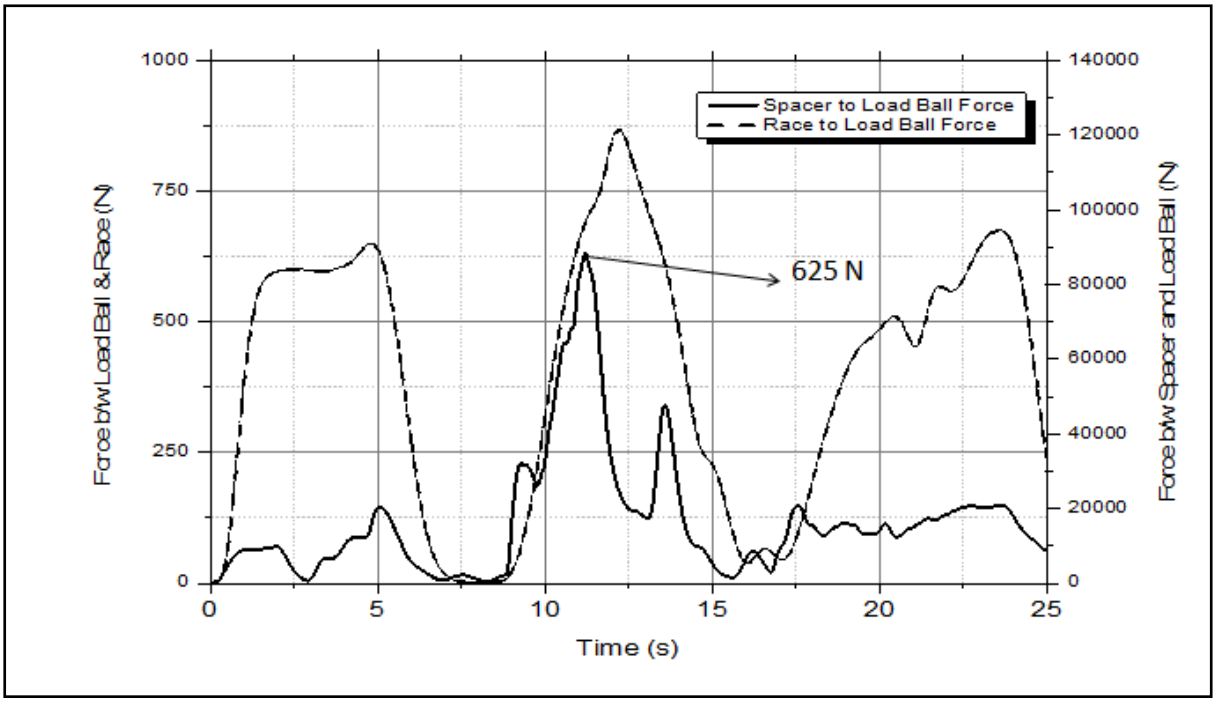

Figure 33: Contact force between the load and spacer ball during bearing operation. Maximum load is 625 N

4.1.2 Parametric Study on Undulation Height

A parametric study was performed with the dia. two meter reduced diameter bearing as modeled in chapter 3. Two undulation profiles are created by increasing and decreasing undulation height magnitudes by 50% to create profiles as shown in Figure 34.

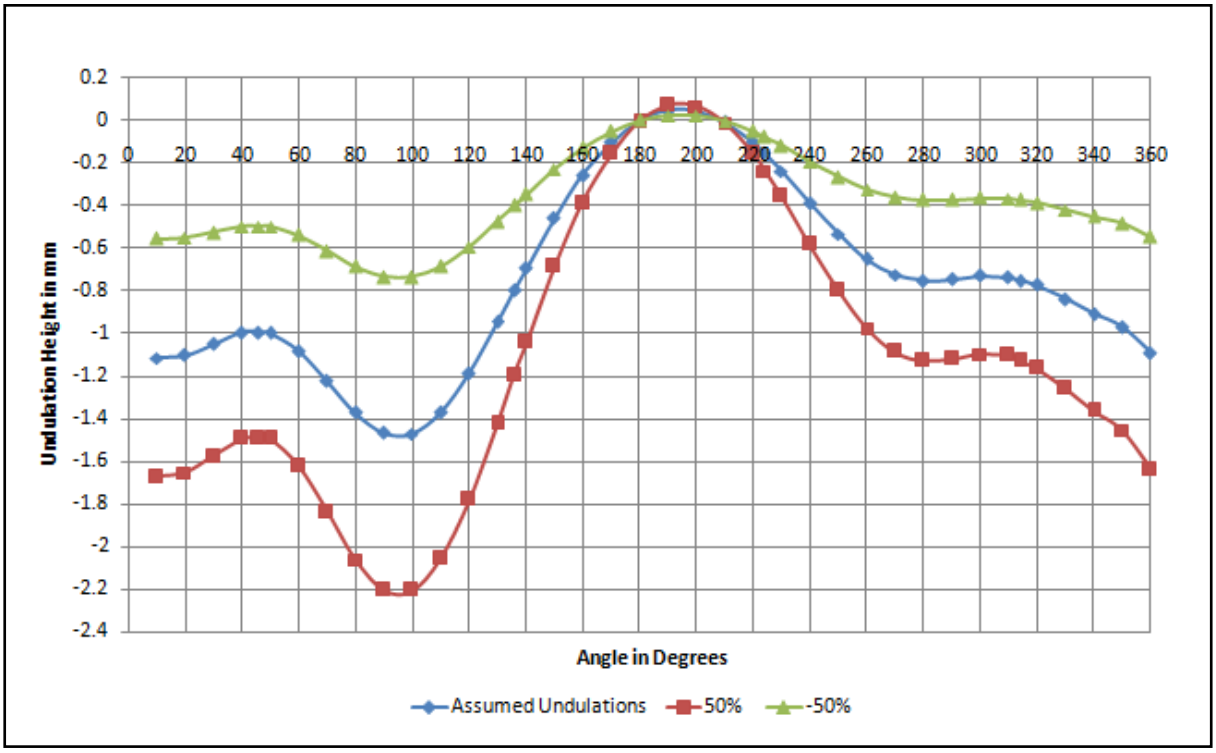

Figure 34: Undulation Profiles used in Parametric Study

Load distributions obtained with parametric study are presented below in Figure 35. Following are the observations.

1. Maximum load under each case of undulation profile with original assumption, +50% and -50% and are 12 ton, 16.28 ton and10.6 ton respectively. There is a significant increase in the maximum load.
2. It is observed that as the magnitude of undulation height increases, the number of balls that lost contact with top race or balls in zero load zones also increases. Number balls in no load zone are 7, 10 and 2 for nominal, +50%and -50% undulation heights respectively.

3. Increase in the number of balls in zero load zone with +50% undulation height model is due to the loss of contact between top race and bearing balls for a wider circumference at the undulation location and the bending of top race is not sufficient enough to make contact with the balls.
4. In case of -50% undulation height model, load balls in the undulation pit at ball numbers 7 to 13 are under non-zero load zone in contrast to the case of +50% undulation height model. This is because with the less undulation height, the bending of the top race is sufficient enough to make contact with load balls resulting in non-zero load zone.
5. At ball numbers 23 & 25, zero load zone is observed even with -50% undulation height model as the sector length over which undulation acts is less making it difficult for the top race to bend and make contact with these balls.

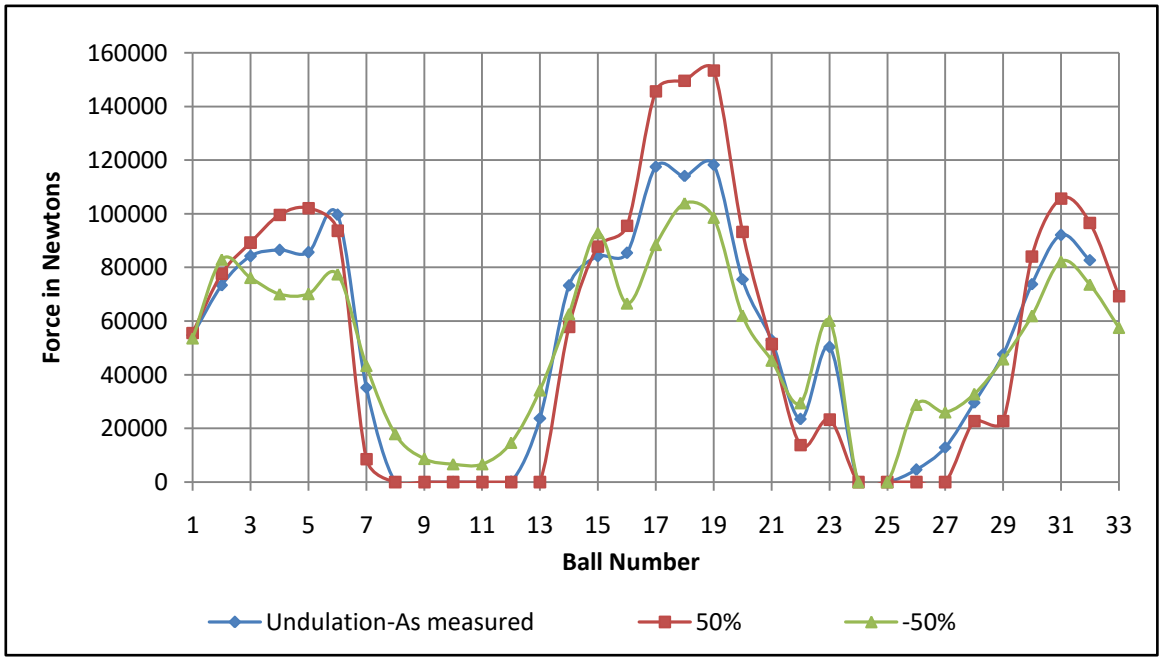

Figure 35: Parametric Study on Load Distribution under the Influence of Undulations. Maximum Loads are 16.28 ton, 12 ton, 10.6 ton on Assumed, +50%and -50% Undulation Height Models Respectively

4.2 Effect of Differential Thermal Expansions on Load Distribution in Bearing

During reactor operation large diameter bearings experience both the axial and circumferential temperature gradients due to the heat transfer from the top shield. In case of axial temperature gradients bottom race and top race experience different temperatures resulting in change in bearing contact angle. A maximum of $20\,^{\circ}C$ axial temperature differences is estimated to occur during reactor operation [23]. This axial temperature gradient will have less impact on the load distribution as it causes a bearing contact angle change uniformly throughout the bearing circumference thus bearing balls experience similar condition throughout its revolution.

Circumferential temperature gradient occurs in the bearing due to the presence of heat exchangers on the reactor top shield which are in hot condition during reactor operation. The locations adjacent to these components experience high temperatures locally resulting in circumferential temperature gradient. Circumferential temperature gradients in the LRP bearing during reactor operation will result in differential radial thermal expansion of bearing races along the circumference. As the bearing rotates, the differential radial expansion leads to misalignments between the bearing top and bottom races of varying magnitude depending on the circumferential distribution of radial thermal expansion of top and bottom races. Influence of these differential thermal expansions on the load distribution is studied parametrically by varying the magnitude of misalignment caused by differential radial thermal expansions.

Effects of differential thermal expansions on the bearing ball are better captured using dynamic analysis as the load variations on the bearing ball are captured in dynamic analysis as the ball moves into the region of misalignment (shown in Figure 36). These effects cannot be captured in static simulations as it simulates load distribution on the bearing ball only at a given instance of time rather than simulating the load variations on the ball during its

movement into differential thermal expansion. MBD analysis capturing the effect of thermal expansion of 0.5 mm on load experienced by three load balls in series is shown in Figure 37.

Further a parametric study is performed to study the effect of increase in thermal expansion. MBD model used in the parametric study on differential thermal expansion is the same two meter diameter bearing with constraints and contact parameters as described in Chapter 3. Since the differential thermal expansion is in radial direction. all the bodies including top race and TMR are modeled as rigid bodies because the bending flexibility of races in radial direction is negligible. Radial thermal expansions of 0.3 mm, 0.4 mm and 0.5 mm corresponds to 7.5°C, 10°C and 12.5°C temperature difference in full scale bearing of Φ6.69 meter. For the study purpose, these misalignments are geometrically modeled in the top race at 90° and 270° locations on the bearing races over a 20° sector from 80° to 100° as shown in Figure 36 to perform parametric study. Parametric study is performed by rotating the top race by two complete rotations in order to revolve all bearing balls by at least one complete revolution along the bearing circumference. Load experienced by the load ball under the influence of differential thermal expansions are presented in Figure 37 and 38.

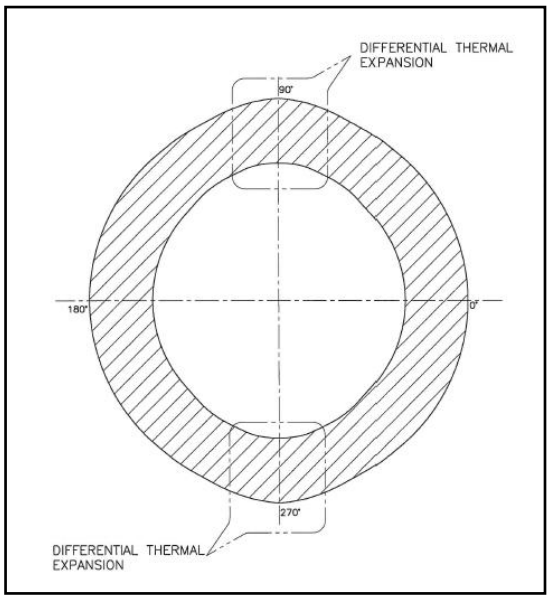

Figure 36: Schematic Diagram of Differential Thermal Expansion Locations Geometrically Modelled on Bearing Top and Bottom Races

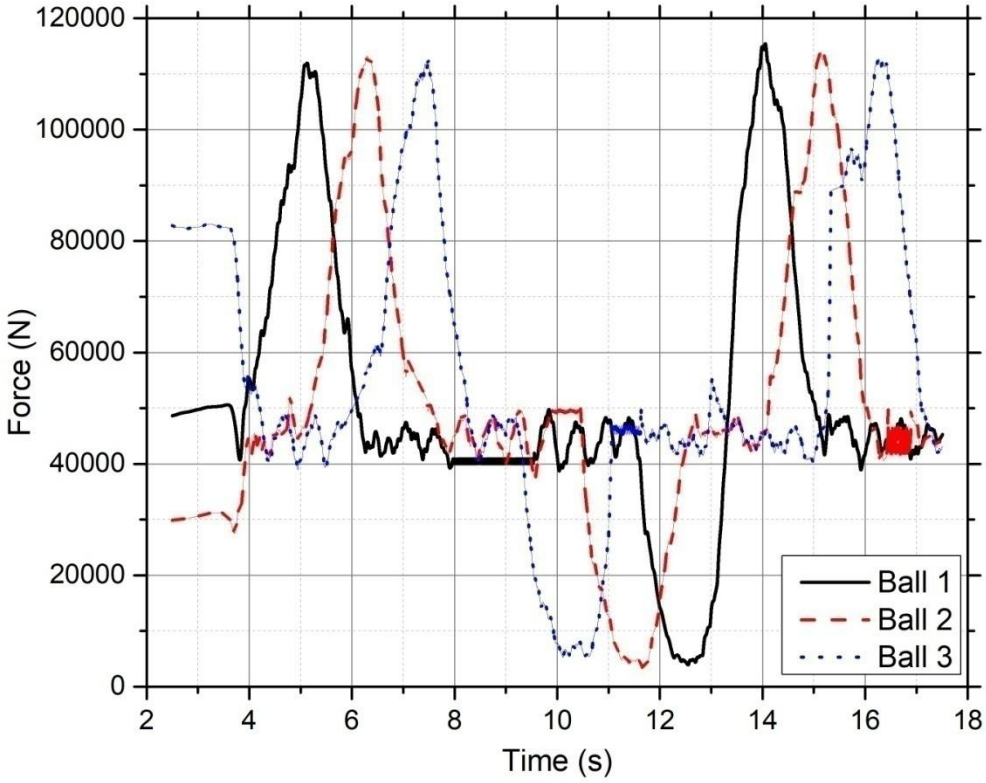

Figure 37: Figure Showing the increase and decrease in the load experienced by the load ball as it travels through 0.5 mm thermal expansion region.

Following are the observations from the results plotted in Figure 37 and 38.

1. It is observed that load balls experience maximum load when ball enters the misalignment region where thermal expansion is present on the top race and bottom race is not expanded. This is due the decreased gap between the races resulting in decreased contact angle of the bearing and increased load on the ball.
2. In regions where no misalignments are present, balls experience a uniform load of 4.24 ton (observed in bearing with no undulations).
3. Ball is found to experience less amount of force when the misalignment due to thermal expansion is present on bottom race and top race has no thermal expansion. As the ball

enters the thermal expansion region of bottom race the contact angle of the ball increases thus load on the ball decreases.

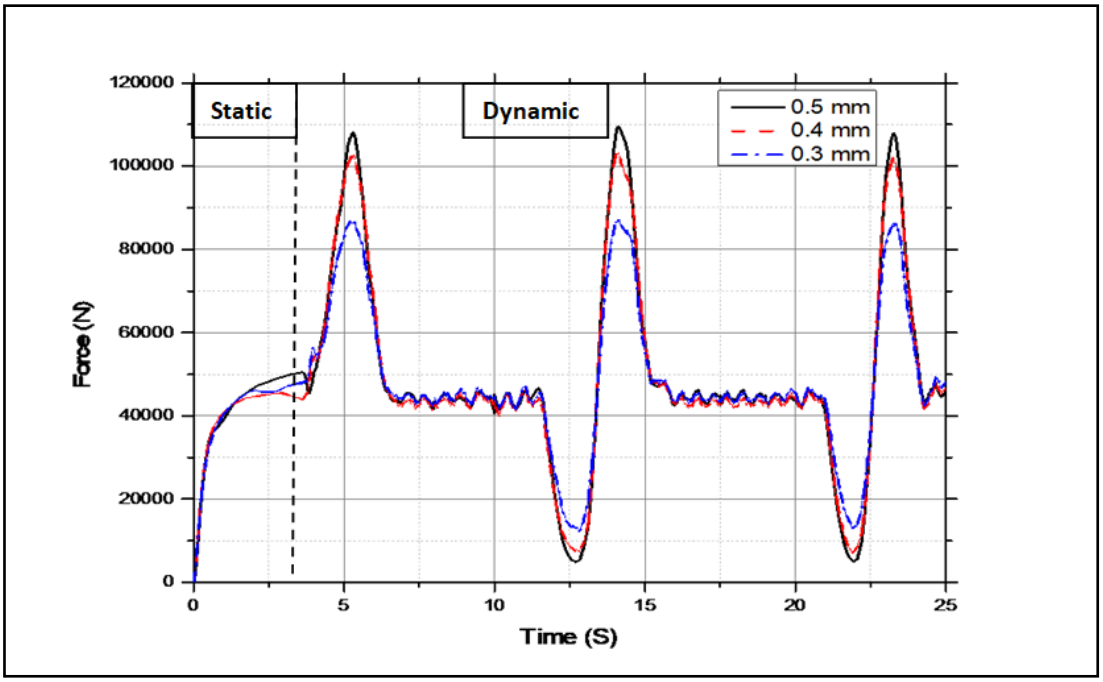

Figure 38: Parametric Study on Load Experienced by a Bearing Ball when rotated by One Rotation under the Influence of Differential Thermal Expansions.

4. From Figure 38 it is observed that load increases on the ball with increase in the height of differential radial thermal expansion. Maximum loads experienced by the load ball are 8.8 ton, 10.4 ton and 11.3 ton due to 0.3 mm, 0.4 mm and 0.5 mm differential thermal expansions respectively. The radial contraction of space between the bearings is responsible for increased load is shown in Figure 39 below.
5. Load ball to spacer ball contact force is found to be a maximum of 6 N (Ref. Figure 40) which is small when compared to contact force due to undulations created by differential temperature distribution.

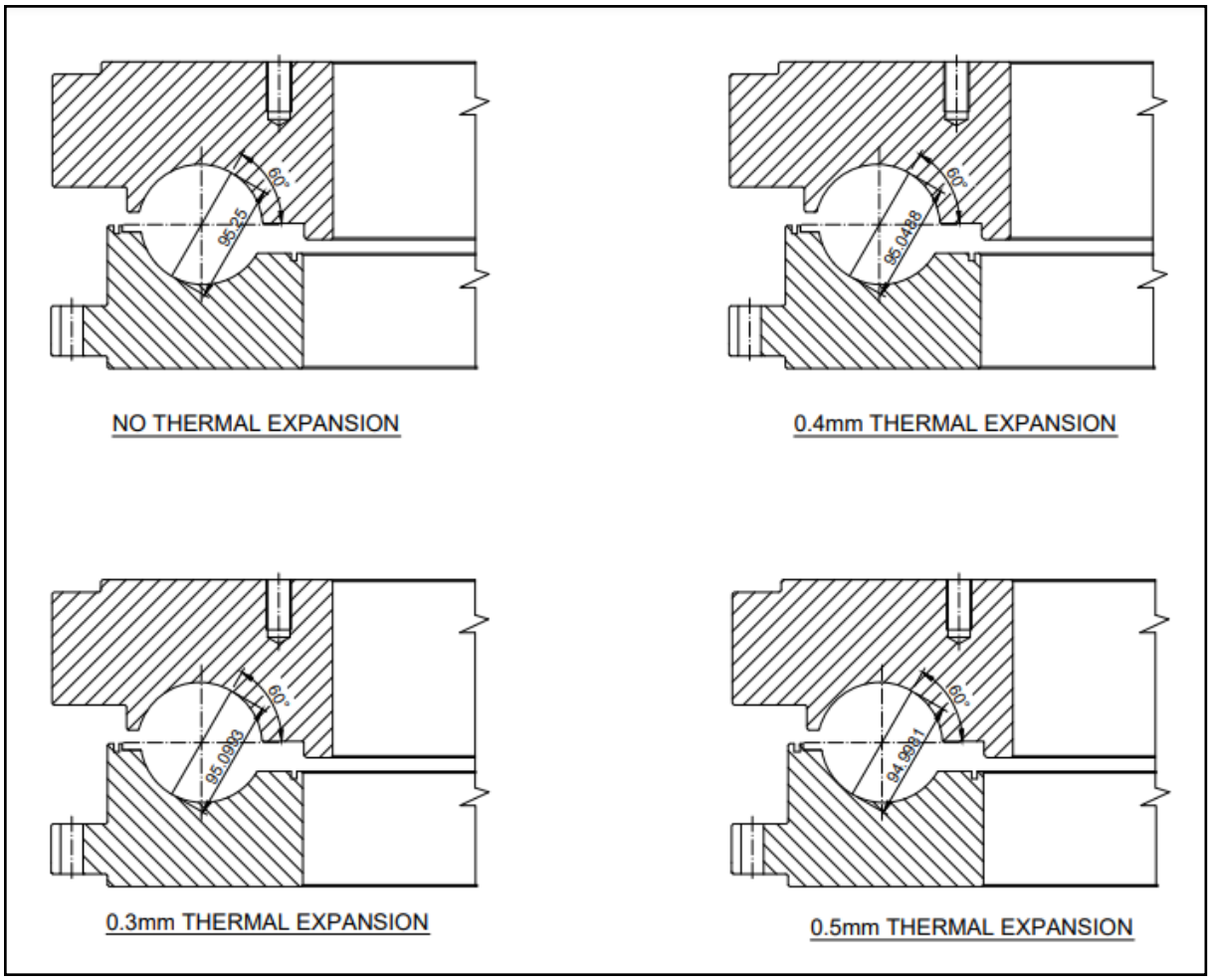

Figure 39: Figures showing the Decreased Gap between the Bearing Races due to Misalignments caused due to Thermal Expansions.

4.3 Effect of Combined Thermal and Undulations on Load Distribution in Bearing

Individual influence of undulations and differential thermal expansions along circumference on the load distribution in the bearing is discussed in sections 4.1 and 4.2. The combined influence of undulations and differential thermal expansions on the load distribution is studied by geometrically modelling these undulations in the baring races. Initially a dynamic simulation with differential thermal expansion height of 0.5 mm and undulations (as shown in Figure 6) modelled in the bearing races is performed. Differential thermal expansions of magnitude 0.5 mm are modelled in top and bottom races at locations as

shown in Figure 35. Undulations are geometrically modelled in the bottom race. Two simulations are conducted, one with inherent stiffness and the other with reduced stiffness. Constraints and contact parameters are same as those discussed in Chapter 3.

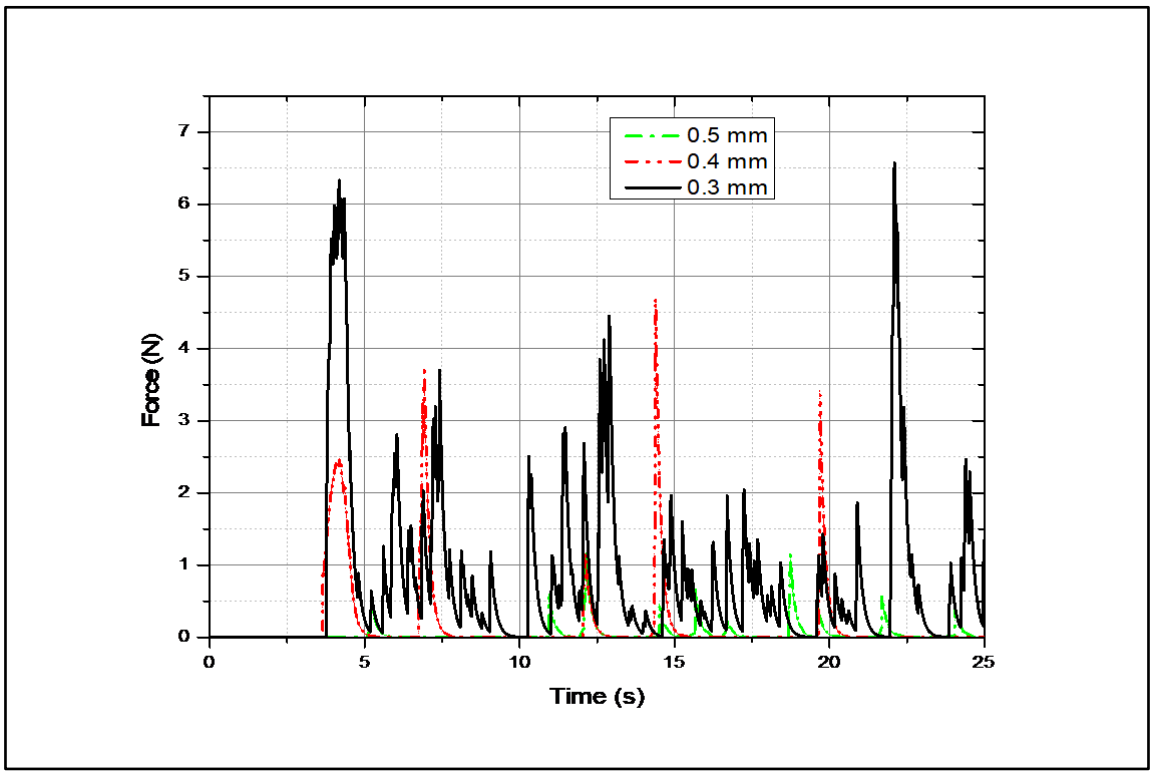

Figure 40: Parametric Study on Contact Force between Load Ball and Spacer Ball under the Influence of Differential thermal expansions. Maximum Contact Force is 6 N

Simulation is performed for a period of 25 seconds so as to rotate the bearing top race by two revolutions resulting in one full revolution of bearing balls. The load ball at the maximum differential temperature location (between top and bottom race) and maximum undulation height location will experience maximum load. Load experienced by such ball is extracted and plotted in Figure 41 and 42 for both the inherent stiffness and reduced stiffness model, respectively.

A design requirement of maximum circumferential temperature difference of 10°C is specified in bearing specification. This requirement is based on the maximum extent to which temperature difference can be controlled on bearing race during reactor operation.

This temperature difference corresponds to a maximum misalignment of 0.4 mm as calculated below.

Radial Thermal expansion = $R\alpha\ \Delta T$ = 0.41 mm

Where R= 3345 mm,α = 12.4e-6 K^{-1},ΔT = 10 K.

Assuming a circumferential temperature gradient of 30°C and 10°C which corresponds to 1.11 mm and 0.41 mm differential thermal expansion respectively, the analysis is repeated in combination with undulations profile as presented in Figure 6.Differential thermal expansions of magnitude 1.11 mm and 0.4 mm are modelled in top and bottom races at locations as shown in Figure 35. Undulations are geometrically modelled in the bottom race. Constraints and contact parameters are same as those discussed in Chapter 3.A dynamic simulation is performed and the maximum load experienced by such ball is identified and shown in Figure 43.

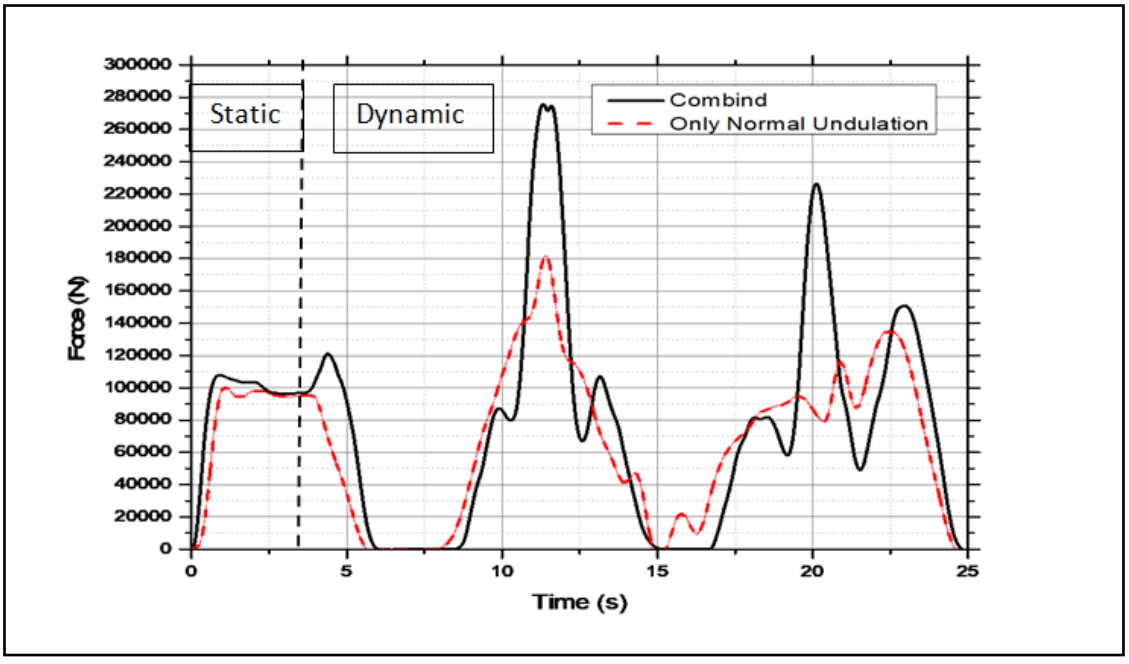

Figure 41: Maximum Load Experienced by Load Ball - Top race and TMR Modelled with Inherent Stiffness. Maximum Load is 28 ton

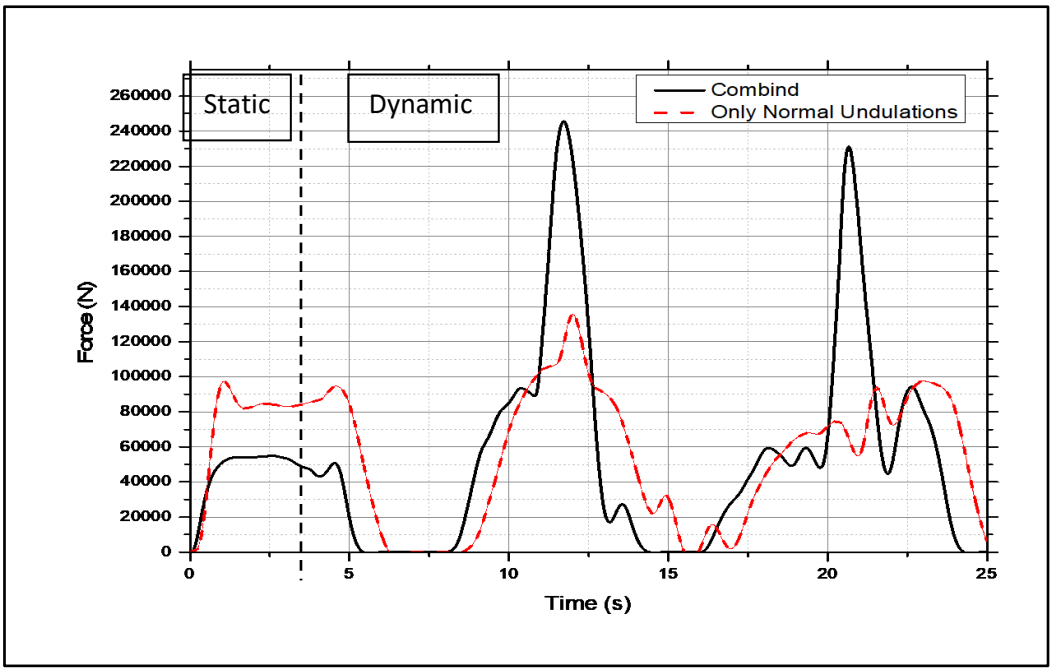

Figure 42: Maximum Load Experienced by Load Ball under the Combined Influence of 0.5 mm Differential Thermal Expansions and Undulations - Maximum Load is 24.5 ton

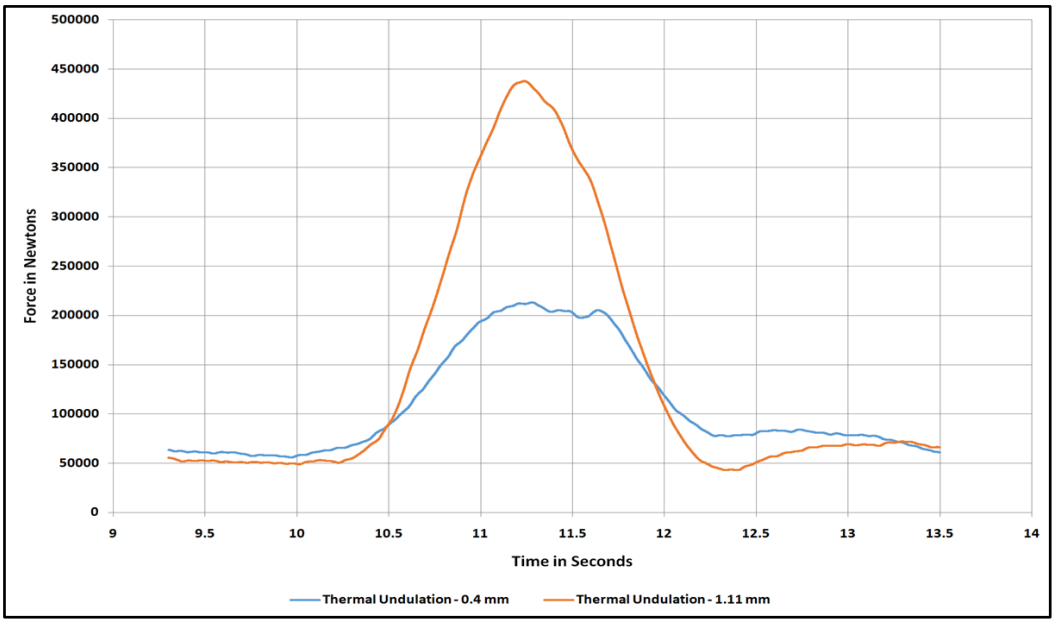

Figure 43: Maximum Load Experienced by Load Ball under the Combined Influence of 1.11 mm and 0.4 mm Differential Thermal Expansion and Undulations - Maximum Loads are 43.8 and 21.4 ton

Above results are conservative as the loads are estimated under simultaneous action of maximum thermal and undulation heights. These loads are expected to occur when maximum misalignment between top and bottom race coincide with maximum undulation height, which is generally rare. The variation in the graphs 42 and 43 at peak load position is due to the curve filtering at different time ranges. This variation can be ignored.

Conservative estimate of maximum load acting through a bearing element in the bearing under the influence of differential thermal expansion misalignment of 1.11 mm and undulations is found to be 43.8 ton. Conservative estimate of maximum load in the bearing under the influence of differential thermal expansion misalignment of 0.4 mm corresponding to 10ºC circumferential temperature variation and undulations is found to be 21.4 ton. Under this load, the contact stresses are expected to be very high and hence, the bearing races are to be induction hardened to sufficient hardness depth to avoid core crushing failure. Estimation of case hardness depth to be achieved to prevent core crushing failure on the bearing races is discussed in section 4.4.

4.4 Estimation of Fatigue Life of Large Diameter Bearing Races under the Influence of Undulations and Differential Thermal Expansions

Under the influence of undulations in the bearing support and differential thermal expansion between the races as discussed above, uneven load distribution is expected in the bearing which results in excessive load on the rolling elements. This excessive load can cause failure of bearing if sufficient case hardness profile is not available on the bearing raceways. Thus, it is essential to estimate the minimum case hardness depth required on the bearings raceways. Methods to estimate required minimum case hardness depth are discussed in detail in section 2.5 of literature survey. These methods are used in estimation of case hardness depth required in Hertzian contact under the loads estimated in section 4.3.Hertzian contact is shown in Figure 44.

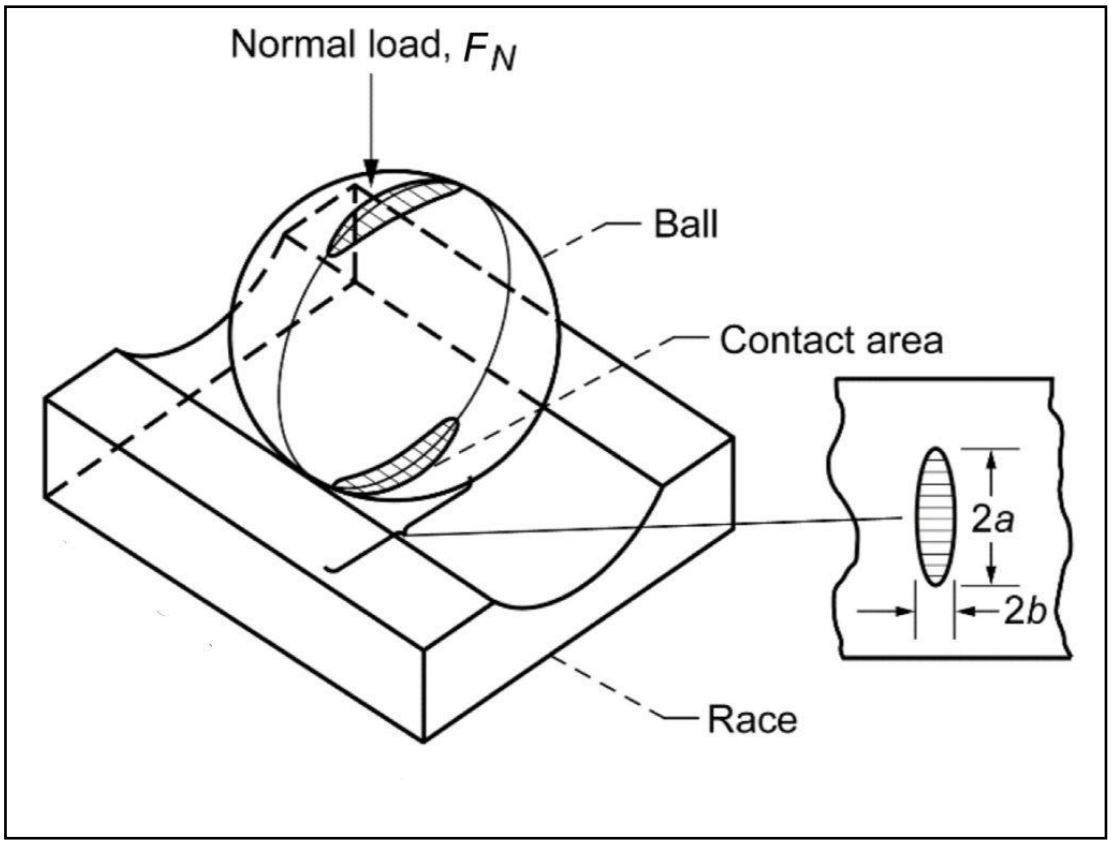

Figure 44: Hertzian Contact between Bearing Ball and Race. Major and Minor Axis Lengths are denoted by a and b of Elastic Deformation at Contact

4.4.1 Estimation of Subsurface Shear Stress Profile on Bearing Races

As per the method discussed in 2.2 a computer code is developed in Python to calculate subsurface shear stress for a given load on the bearing race. Along with sub surface stresses, the code gives Hertzian contact parameters such as dimensions of elastic deformation, maximum contact pressure, depth of maximum shear stress and case hardness depth required. The computer code is attached in Annexure-1.Sample subsurface shear stress distributions plotted by the code in the bearing race under different loads are presented below in Figures 45,46,47,48 and 49. Materials used in the hardness depth calculations are AISI 52100 and AISI 4140 material for bearing ball and bearing race respectively. Material properties used in the calculations are listed in Table 7.

Table 7: Material Properties of Ball and Race [25]

Material Properties	Ball Material (AISI 52100 - Through Hardened to 62 HR_C)	Bearing Material (AISI 4140)
Young's Modulus	207 GPa	207 GPa
Poisson's Ratio	0.29	0.29
Yield Stress	2034 MPa	660 MPa
Ultimate Tensile Stress	2240 MPa	800 MPa

From the stress distributions shown in Figures below, it is observed that maximum shear stress in Hertzian contact increases from surface to a peak value below the race surface and then decrease with increasing depth. Herzian contact parameters at different loads calculated using the code is presented in Table 8.

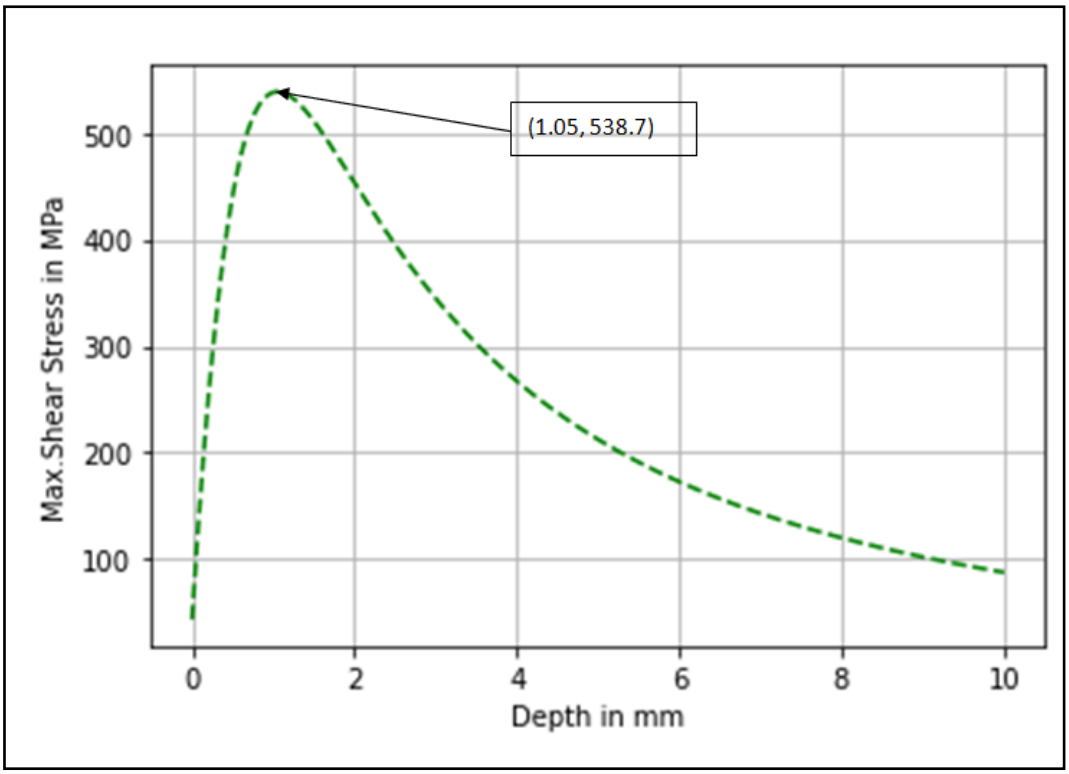

Figure 45: Subsurface Shear Stress Distribution along the Bearing Race Depth under 5 ton Load on Load Ball

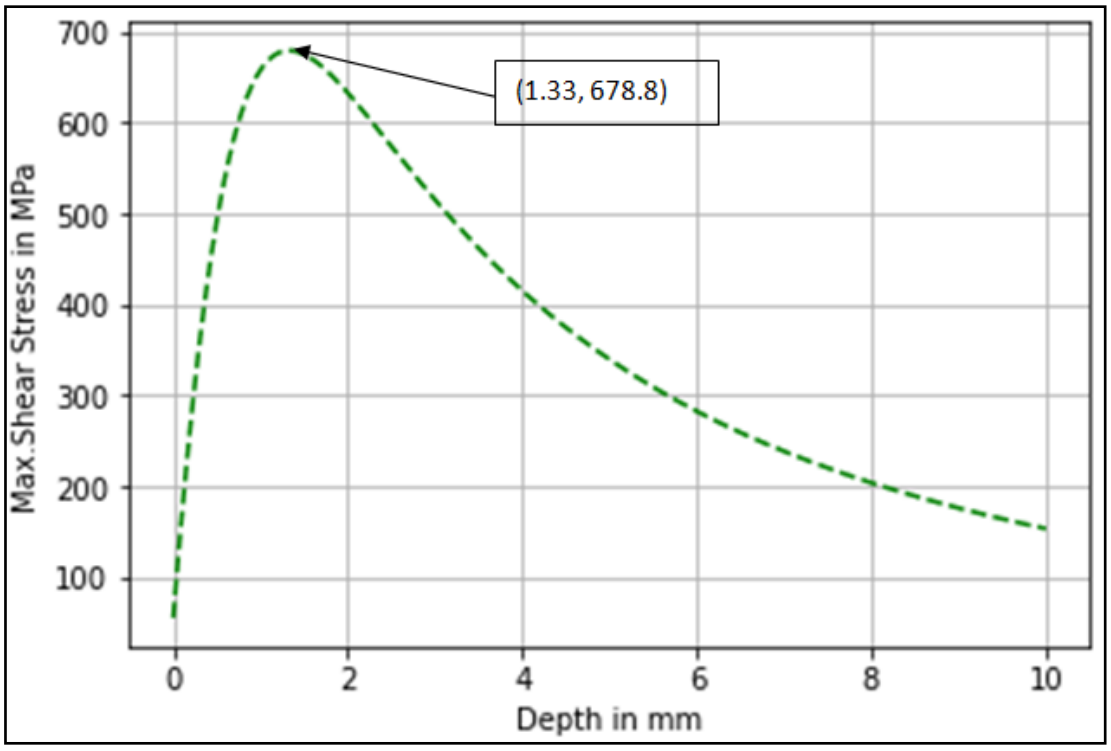

Figure 46: Subsurface Shear Stress Distribution along the Bearing Race Depth under 10 ton Load on Load Ball

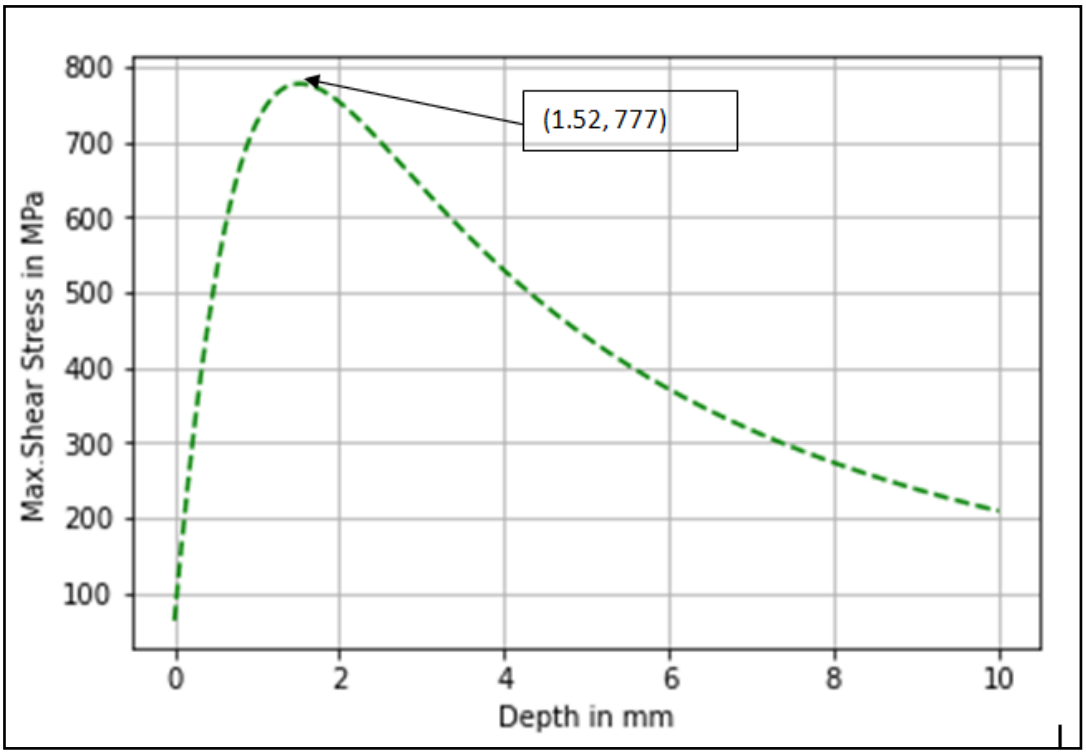

Figure 47: Subsurface Shear Stress Distribution along the Bearing Race Depth at 15 ton Load on Load Ball

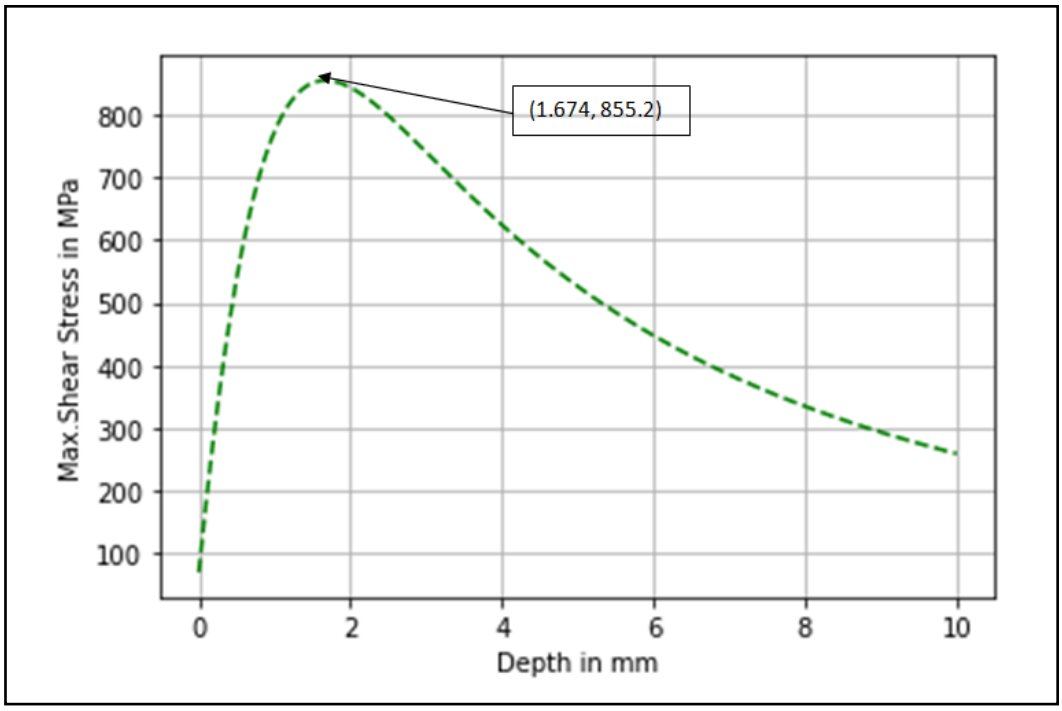

Figure 48: Subsurface Shear Stress Distribution along the Bearing Race Depth at 20 ton Load on Load Ball. Max

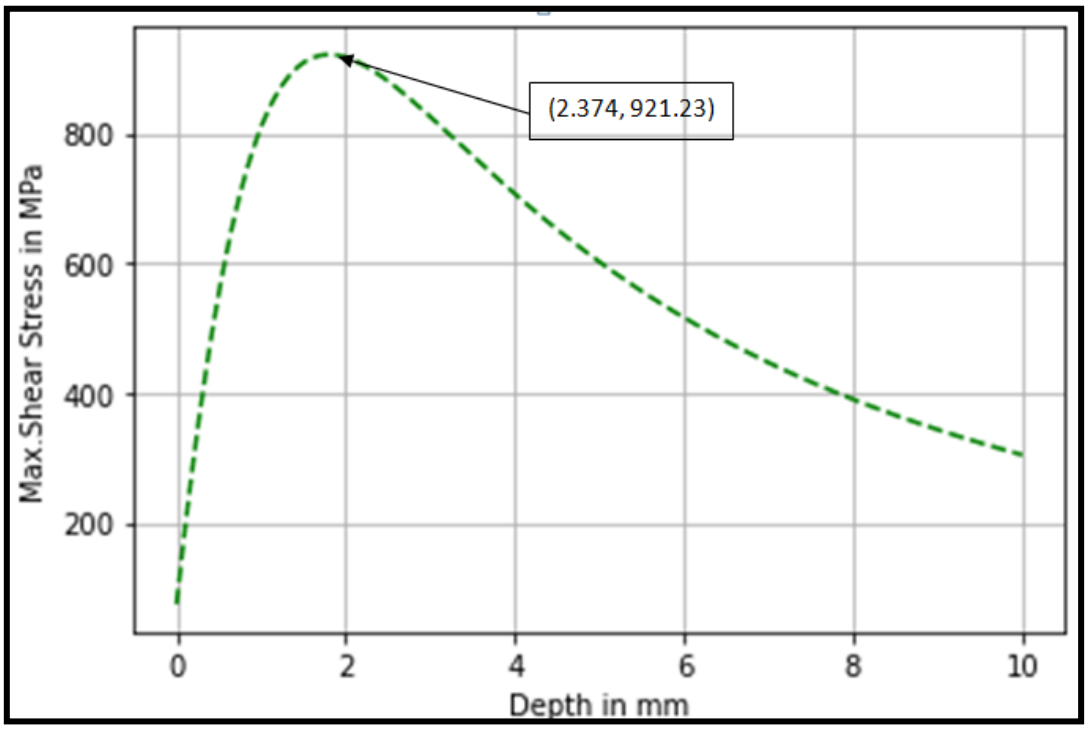

Figure 49: Subsurface Shear Stress Distribution along the Bearing Race Depth at 25 ton Load on Load Ball

Table 8: Parameters of Hertzian Contact at Different Loads

Load on Load Ball	Contact Pressure (MPa)	Max. Shear Stress (MPa)	Max. Shear Stress Depth (mm)	Elastic Deformation - Ellipse	
				Major Axis Length (mm)	Minor Axis Length (mm)
5 ton	1689.7	538.7	1.05	9.97	1.40
10 ton	2128.9	678.8	1.33	12.57	1.75
15 ton	2437.0	777	1.52	14.4	2.00
20 ton	2682.2	855.2	1.67	15.84	2.20
25 ton	2889.3	921.2	1.8	17.05	2.37

4.4.2 Estimation of Fatigue Life of Bearing

The code used in plotting subsurface shear stresses is modified to estimate the fatigue life as per the criteria discussed in literature survey (section 2.5). This code is also presented in Annexure 1.

Damage caused due to material fatigue is considered in estimating dynamic capacity and L_{10} life of the bearing using ISO 281 standard. But this standard pertains to bearing manufactured from AISI 52100 steel through hardened to at least a minimum of 58HR_C. So, an estimate of fatigue life of the bearing considering achievable case hardness profile of the bearing is necessary. Based on the "Wind Turbine Design Guidelines DG03: Yaw and Pitch Rolling Bearing Life" given by National Renewable Energy Laboratory (USA) [3], an estimate of fatigue life of large size bearing is calculated. Detailed Procedure is discussed in section 2.5.

Fatigue strength in shear of the AISI 4140 material as per Ref.25 is presented below.

Yield Strength	=	660 MPa
Yield Strength in Shear	=	330 MPa
Fatigue Strength in Shear	=	198 MPa

I. Fatigue Life under Maximum Load of 4.24 ton

Uniform distribution of load is observed on the bearing balls under the ideal condition of no undulations and no differential thermal expansions in the bearing races.

ISO life of the LRP bearing as per ISO 281 -2007 standards is calculated as per section 2.5:

1. Calculation of Dynamic Rating of the Bearing (C_a)

$$C_a = 3.647 b_m f_c (\cos\alpha)^{0.7} \tan\alpha \, Z^{\frac{2}{3}} D_b^{1.4} = 1950868 \text{ N}$$

Where,

D_b = Diameter of the Bearing Ball = 95.25 mm

Z= no of load balls = 116

α = Angle of bearing = 60°

b_m = Factor to take the contemporary good manufacturing practices of hardened bearing steel = 1.3

In order to obtain a conservative estimate of ISO life b_m is taken as 1 instead of 1.3.

f_c = Value obtained from the Table 4 of ISO 281 code = 36.635

2. Calculate ISO bearing fatigue life using equation below

P_a = Equivalent Axial load on the bearing =5.874×10^6 N Ref. 23

$$L_{10}\ life = (\frac{C_a}{P_a})^3 = 0.036633 \text{ Million revolutions}$$

$$L_{10} \text{ Life} = 36633 \text{ Revolutions}$$

Under this condition, for a large diameter bearing to have fatigue life equal to that of ISO life as calculated using ISO 281 standard, sufficient case hardness depth on the bearing race is to be provided to make fatigue life correction factor equal to 1.

$$A_{cd} = \frac{\text{Fatigue Shear Strength in Fatigue}}{\text{Shear Stress at Hardened Case to Core Material Interface}}$$

Load on the individual bearing ball under uniform distribution is 4.42 ton, case hardness depth corresponding to fatigue life equal to ISO life is found to be 4.8 mm as shown in Figure 50.

II. Fatigue Life under Maximum load of 21.4 ton

For the case of undulations and misalignment of 0.41 mm, maximum load on a given bearing ball is found to be 21.4 ton. Under this load, subsurface shear stress profile and the fatigue life correction factor is calculated taking the case hardness depth on bearing races equal to the case hardness depth required for uniform load distribution (as plotted in Fig. 52). In Figure 52, it can be observed that in order to have bearing life equal to ISO life a hardness depth of 12.5 mm is required.

Similar fatigue life calculation is performed for 43.8 ton load and fatigue life is found to be 8425 revolutions as shown in Figure 51.

Max. shear stress at hardened case-core interface (4.8 mm)	=	854.32 MPa
A_{cd}	=	0.35
Fatigue Life	=	12821 Revolutions

The fatigue life calculated above has large amounts of conservatism built into it due to following reasons.

1. The peak load used in the fatigue life calculations are obtained from the case of both the thermal misalignments and the maximum undulation heights are coinciding with each other.
2. The peak load used in the calculation acts only on one ball at a given time. The design guidlines used for calculation of factor A_{cd} gives the same fatigue life even when all the balls experience same amount of peak load. Thus there is an inbuilt conservatism built in the calculation itself.
3. The calculation of ISO life as per ISO 281-2007 standard is a conservative estimate as the factor b_m value is reduced intentionally to 1 from 1.3.

Thus the fatigue life values are higly conservative estimates, thus beargings are expected to have life greater than the above mentioned values.

4.5 Summary

Results and discussion on individual influence of undulations and differential thermal expansions are presented. The combined effect of undulations and differential thermal expansions is also discussed by conservatively estimating maximum load on load balls. These estimates are used to estimate the bearing fatigue life by calculation of fatigue life correction factor. From the above results, it is found that under the influence of undulations, bearing fatigue life is reduced to less than half of ISO fatigue life as specified by ISO 281 standard.

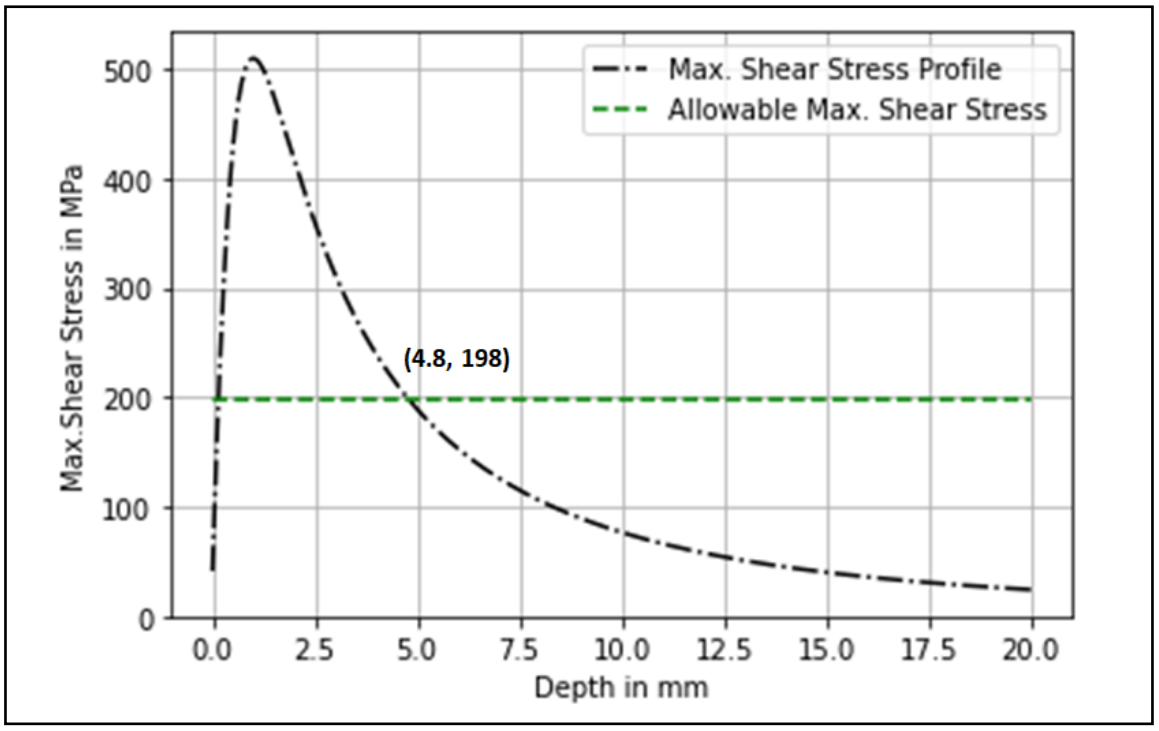

Figure 50: Subsurface shear stress profile in bearing race under the influence of 4.24 ton load.

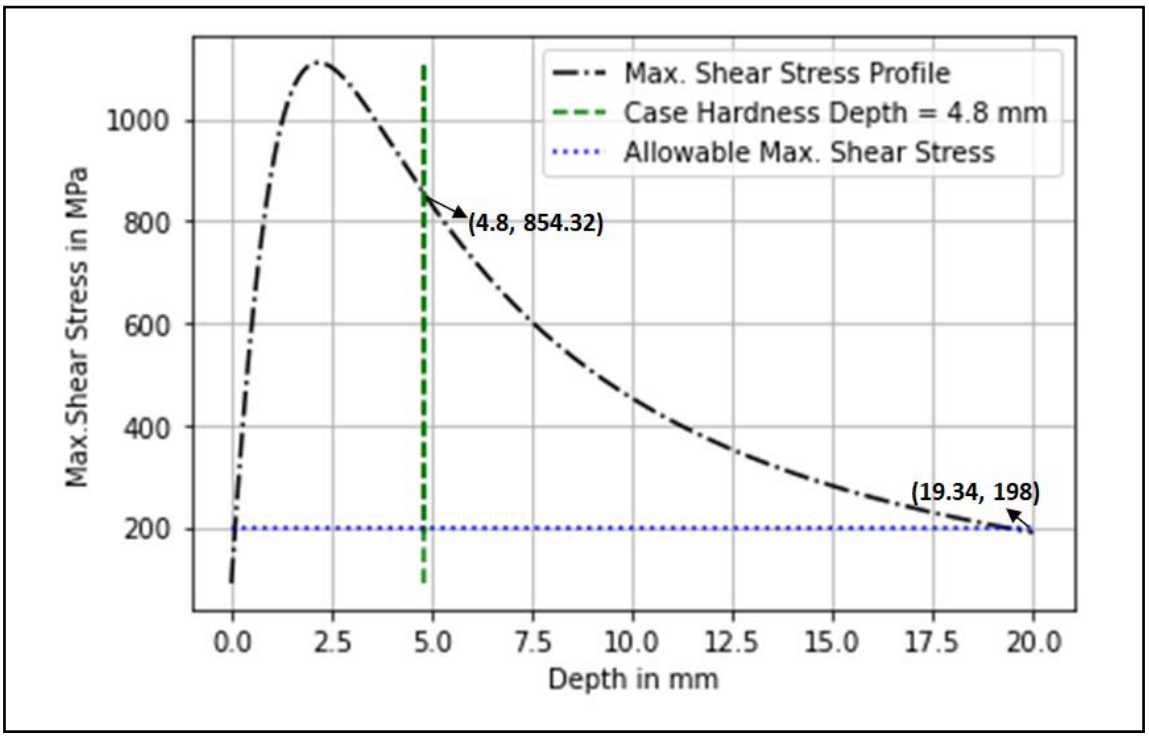

Figure 51: Subsurface shear stress profile in bearing race under the influence of 43.8 ton load.

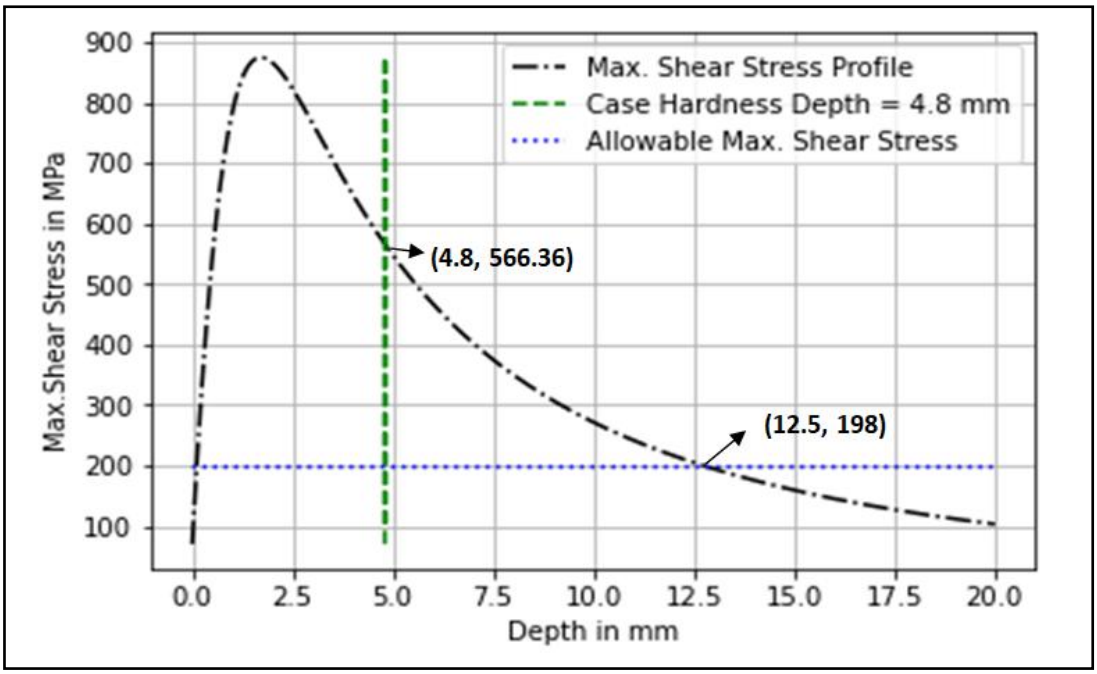

Figure 52: Subsurface shear stress profile in bearing race under the influence of 21.4 on load.

CHAPTER 5

SUMMARY AND CONCLUSIONS

5.1 Results Summary

The effect of undulations and circumferential temperature gradient on the performance of large diameter bearing is estimated. Initially the MBD simulation tool is validated to perform dynamic analysis on the bearing. Then the individual effect of undulations and circumferential temperature gradient are estimated to obtain the maximum load experienced by the rolling elements. Followed by this, combined effect of undulations and thermal misalignments is studied to obtain the conservative estimates of fatigue life of the bearing.

Summary of results are presented in the Table 9.

Table 9: Summary of Results

Model	Results
Maximum load on a ball due to undulation formed by elastic deformation – Inherent Stiffness 2 meter Model	163.73kN(16.7 ton)
Maximum Load due to undulation formed by elastic deformation of support structure (undulations) – Reduced Stiffness 2 meter Model	118.3kN(12 ton)
Maximum load on a ball due to differential thermal expansion of (0.5mm,0.4mm,0.3mm)	110.60 kN,101.7 kN,86.42 kN (11 .3 ton, 10.37 ton, 8.8 ton)

Maximum load on a ball due to undulations of height X, 1.5 X and 0.5X where X is 1 mm	118.3kN,159.7kN,103.97kN (12 ton, 16.3 ton, 10.6 ton)
Maximum load on a ball Combined interaction of undulations and 1.11 mm differential thermal expansion – Corrected stiffness model	429.5 kN (43.8 ton)
Combined interaction of undulations and 0.4 mm differential thermal expansion – Corrected stiffness model	210.2 kN (21.4 ton)
ISO life of bearing at uniformly distributed load of 4.24 ton	36633 Revolutions
Fatigue life under maximum load of 21.4 ton	35% of ISO Life 12821 Revolutions
Fatigue life under maximum load of 43. ton	23% of ISO Life 8425 Revolutions

5.2 Conclusions

1. Procedure to study effects of undulations and Differential thermal expansions using multi body dynamics (MBD) simulations is established.

2. Validation of commercial multipurpose MBD software - Recurdyn - to estimate bearing load distribution under the influence of undulations is established.

3. Procedure to model full scale Φ6.69 bearing stiffness in Φ2 meter bearing model is established. This reduces computational time.

4. Load distribution in the bearing under the individual influence of undulations and differential thermal expansions and combined undulations are obtained.

5. Based on the results obtained with dia. 2 m bearing, the maximum load on the ball in full size bearing of dia. 6.69 m under the influence of undulations is found to be 12 ton. Maximum ball to ball interaction force is found to be 625N, which is found to be small.

6. Maximum load on the ball in the bearing under influence of differential thermal expansion misalignment of 0.4 mm (corresponding to 10ºC circumferential temperature variation along the races) alone is found to be 10.4 ton.

7. Maximum load on the ball in the bearing under the influence of differential thermal expansion misalignment of 1.11 mm (max. assumed misalignment) and undulations is found to be 43.8 ton.

8. Maximum load on the ball in the bearing under the influence of differential thermal expansion misalignment of 0.4 mm (corresponding to 10ºC circumferential temperature variation) and assumed undulation profile is found to be 21.4 ton.

9. Spacer ball to load ball interaction force is found to be low at 860 N under the combined effect of undulations and differential thermal expansions.

10. Fatigue life of the bearing is calculated as per ISO 281-2007 standard under the uniform loading condition of 4.24 ton. The calculate fatigue life is 36633 revolutions.

11. Under the influence of undulations and differential thermal expansions, fatigue life is reduced considerably as shown in section 4.4. Fatigue life is 23% and 35% of ISO fatigue life under the maximum load of 43.8 and 21.4 tons respectively. This confirms that the circumferential temperature difference needs to be controlled.

5.3 Future Works

1. Simulation of dynamic analysis of full scale large diameter bearing.
2. A dynamic analysis of bearing with ball spacer or cage concept instead of spacer balls to study the kinematic and dynamic behavior of ball spacers.
3. Dynamic analysis to study the effect of bearing lip seals on the drive torques.

REFERENCES

1. **Changsen,W.**(1991), Analysis of Rolling Element Bearings, *Mechanical Engineering Publications Ltd., London,* Ch.3

2. **Howard R. Thomas, Victor A. Hoersch** (2007), Station Stresses Due to the Pressure of on Elastic Solid Upon Another with Special Reference to Railroad Rails, *The Engineering Experiment Station, University of Illinois.*

3. **Bearing Damage and Failure Analysis**. SKF bearings.

4. **Oskar Zwirien and Walter P. Wleland**,(1983) Case Depth for Induction Hardened Slewing Rings, *SAE Technical Paper Series*831271

5. **Smolnicki, Tadeusz, Stańco, Mariusz and Pietrusiak, Damian**. (2013). Distribution of loads in the large size bearing - Problems of identification. *TehnickiVjesnik.* 20. 831-836.

6. **Sriramachandra Aithal, N Siva Prasad, et al,** Effects of Manufacturing Errors in large diameter slewing bearings of fast breeder reactor rotating plug,*Journal of Mechanical Engineering Science* 2015

7. **Ost, W. and de baets, Patrick and De Waele, Wim.** (2004). Failure of a large ball bearing of a dockside crane. Engineering Failure Analysis - *ENG FAIL ANAL. 11. 335-353. 10.1016/j.engfailanal.*2003.08.006.

8. **Nagatomo, T., K. Takahashi, Y. Okamura, T. Kigawa and S. Noguchi** (2012), Effects of load distribution on life of radial roller bearings, *Transactions of ASME – Journal of Tribology,* 134, 021101-1 to 021101-7.

9. **Potocnik, R., P. Goncz, J. Flasker and S. Glodez** (2010), Fatigue life of double row slewing ball bearing with irregular geometry, *Procedia Engineering*, 2, 1877-1886

10. **Potocnik, R., P. Goncz, J. Flasker and S. Glodez** (2013), Static capacity of large double row slewing ball bearing with predefined irregular geometry, *Mechanism and Machine Theory*, 64, 67-69.

11. **Liu, X.; Liu, D.; Hu, X.**(2021) Influence of the Bearing Thermal Deformation on Nonlinear Dynamic Characteristics of an Electric Drive Helical Gear System. *Sensors, 21*, 309.

12. **Mitrovic, M., Radivoje and Atanasovska, Ivana and Soldat, Natasa and Momcilovic, Dejan**. (2015). Effects of operation temperature on thermal expansion and main parameters of radial ball bearings. *Thermal Science*. 19. 91-91.

13. **LudwikKania**, (2006) Modelling of rollers in calculation of slewing bearing with the use of finite elements, *Mechanism and Machine Theory*, Vol-41, Issue-11, Pages 1359-1376.

14. **X H Gao, X D Huang, H Wang and J Chen**, (2011) Modelling of ball-raceway contacts in a slewing bearing with non-linear springs, *Journal of Mechanical Engineering Science*, Vol-225, Issue 4.

15. **ISO 281:2007,** Rolling Bearings - Dynamic Load Ratings and Rating Life, *International Organization for Standardization.*

16. **T. Harris J.H. Rumbarger C.P. Butterfield**, (2009) Wind Turbine Design Guidelines DG03 - Yaw and Pitch Rolling Bearing Life, *National Renewable Energy Laboratory (USA)*.

17. **Rafael Vischi, Carvalho, Katia Lucchesi and Cavalca**, (2009) Dynamic analysis of ball bearing, *SAE technical Paper Series* -2009-36-0057.

18. **Zhaohui, Qi and Wang, Gang and Zhang, Zhigang. (2014).** Contact analysis of deep groove ball bearings in multibody systems. *Multibody System Dynamics*. 33. 115-141. 10.1007/s11044-014-9412-0.

19. **Gao Y, Li Z, Wang J, Li X, An Q. (2013).**Influences of bearing housing deflection on vibration performance of cylinder roller bearing–rotor system. *Proceedings of the Institution of Mechanical Engineers, Part K: Journal of Multi-body Dynamics*. 2013; 227(2):106-114. doi:10.1177/1464419312466216.

20. **Stacke L-E, Fritzson D, Nordling P.** (1999).BEAST—a rolling bearing simulation tool. Proceedings of the Institution of Mechanical Engineers, *Part K: Journal of Multi-body Dynamics*. 1999; 213(2):63-71. doi:10.1243/1464419991544063

21. **Pradeep K. Gupta. (1984)** Advanced Dynamics of Rolling Elements, *Springer Publications.*

22. **Recurdyn.** Multi Body Dynamic Software**,** Release V9R4.

23. **Sriramachandra Aithal. (2007).** Detailed design of large diameter slewing ring bearing for FBR applications, *PFBR Internal Report*, PFBR31300DN1058-A.

24. **Tore Dahlberg,** Procedure to calculate deflections of curved beams, *International Journal of Engineering Education*. Vol. 20, No. 3.

25. **Jagruti Mote, et.al**, Summary of Inspection Reports on LRP Bearing, *PFBR Internal Report*, PFBR/31320/DN1005/Rev-A.

26. **Douglas Godfrey.** (1964) Friction of Greases and Grease Components during Boundary Lubrication. *ASLE TRANSCTIONS*, 7(1):24-31.

27. **ANSYS Multi-physics,** Finite Element Software, V18.2.

28. **AZOM Material –** AISI 4140 Material Properties

ANNEXURE-I

Computer code in python to plot sub-surface shear stress profile in Hertzian contact for a given load as per the algorithm presented in section 2.2.

```
Import numpy as np
Import matplotlib.pyplot as plt
import math as m
import scipy
from scipy import special
'Input Data'
Db=95.25# diameter of ball
Dm=6690# pitch diameter of bearing
alp=1.047619#60deg
sal=510# yeild strength
E1=207e3#ball E
E2=207e3#race E
v1=0.29# poission ratio
v2=0.29
UTS=800
YS=660
Criteria1=0.5*YS #Pallini & Sague Criteria
Criteria2=0.425*UTS#Sauge & Rumbarger Criteria
W=21.4
Qmax=(W*1000*9.81)#/(m.sin(alp)) # Max. load on ball taking
eccentricity into account
Zc=10
print('Load on ball is',W,'ton')
print('Load on the bearing ball is',Qmax,'N')

'Calculation of Curvatures'
r11=2/Db
r12=2/Db
gamma=(Db*m.cos(alp))/Dm#to take effect of contact angel
fi=fo=0.525#this value is selected from the the point of axial
thermal exp. and load bearing capacity
r21=(2/Db)*(gamma/(1-gamma))
```

```
r22=-(1/(fi*Db))
sumr= r11+r12+r21+r22
Fr=abs((r11-r12)+(r21-r22))/sumr#used in calculation of elliptical
contact area dimensions
#print ('Fr is =',Fr)

'Calculation of ellpitical contact dimensions'
#print('ma and mb corresponding to Fr is')
#print('ma=3.233, mb=0.4499')
ma =3.233
mb=0.4499
a= ma*(((1.5*(Qmax/sumr))*(((1-v1**2)/E1)+(1-v2**2)/E2))**(1/3))
b= mb*(((1.5*(Qmax/sumr))*(((1-v1**2)/E1)+(1-v2**2)/E2))**(1/3))
print('Semi Major Axis Length (a) =',a,'mm')
print('Semi Minor Axis Length (b) =',b,'mm')
Po=1.5*(Qmax/((22/7)*a*b))
print('Max. Contact Compressive Stress on Race Surface =',Po)
k=b/a #contact modulus
print('Contact Modulus (b/a) is',k)
e= m.sqrt((1-k*k))#eccentricity of ellipse
#k=0.15
'Calculation of subsurface shear stress'
Ep= scipy.special.ellipe(e**2)
M=(2*k*k)/(e*e*Ep)
L=(2/sumr)*(((1-v1*v1)/E1)+((1-v2*v2)/E2))
z=0
j=0
Shear= np.zeros(int(100000))
Depth= np.zeros(int(100000))
ba= np.zeros(int(100000))
ref1= np.zeros(int(100000))
ref2= np.zeros(int(100000))
while j<100000:
    c=z/a
    t=m.sqrt((k*k+c*c)/(1+c*c))
if z==0:
phi=22/14;
```

```
else:
phi= m.atan(a/z)
    E=scipy.special.ellipeinc(phi,e*e)
    F=scipy.special.ellipkinc(phi,e*e)
    omy1=(1/(2*t))+(1/2)-(t/(k**2))+c*(((1/(k**2))*E)-F)
    omy2=-1+t+c*(F-E)
Syn=M*(omy1+v1*omy2)
Sy=(a/L)*(Syn)
Szn=-((M/2)*((1/t)-t))
Sz=(a/L)*Szn
Ss=0.5*abs(Sy-Sz)
#print(z,Ss)
    Shear[j]=Ss
    Depth[j]=z
ref1[j]=4.8
ref2[j]=198
    z=z+0.0002
    j=j+1
fig= plt.figure()
Line1,= plt.plot(Depth,Shear,'black',linestyle='-.',label="Max.
Shear Stress Profile")
plt.xlabel('Depth in mm')
plt.ylabel('Max.Shear Stress in MPa')
#plt.plot(Depth,Shear)
Line2,= plt.plot(ref1,Shear,'Green',linestyle='--',label="Case
Hardness Depth = 4.8 mm")
Line3,= plt.plot(Depth,ref2,'Blue',linestyle=':',label="Allowable
Max. Shear Stress")
plt.legend(handles=[Line1, Line2, Line3])
plt.grid()
plt.show()
```